eNeuro

Research Article: Confirmation | Disorders of the Nervous System

Circadian and Brain State Modulation of Network Hyperexcitability in Alzheimer's Disease

Rosalind Brown[1], Alice D. Lam[2,3], Alfredo Gonzalez-Sulser[1], Andrew Ying[1], Mary Jones[1], Robert C.-C. Chou[1], Makis Tzioras[1], Crispin Y. Jordan[1], Izabela Jedrasiak-Cape[1], Anne-Laure Hemonnot[4], Maurice Abou Jaoude[3], Andrew J. Cole[2,3], Sydney S. Cash[2,3], Takashi Saito[5], Takaomi Saido[5], Richard R. Ribchester[1], Kevan Hashemi[6] and Iris Oren[1]

[1]*Centre for Discovery Brain Sciences, University of Edinburgh, Edinburgh, UK*
[2]*Epilepsy Division, Massachusetts General Hospital, Boston, MA USA*
[3]*Harvard Medical School, Boston, MA USA*
[4]*Université De Montpellier, Montpellier, France*
[5]*Laboratory for Proteolytic Neuroscience, RIKEN Brain Science Institute, Japan*
[6]*OpenSource Instruments Inc, Watertown, MA USA*

DOI: 10.1523/ENEURO.0426-17.2018

Received: 5 December 2017

Revised: 8 March 2018

Accepted: 6 April 2018

Published: 27 April 2018

Author Contributions: RB, RRR and IO designed research; RB, ADL, AG-S, MJ, RC-CC, IJ-C, A-LH, TS and TS performed research; ADL, AY, RC-CC, MT, CYJ, A-LH and IO analysed the data; MAJ, AJC, SSC and KH contributed unpublished analytical tools; RB, ADL, KH and IO wrote the paper.

Funding: http://doi.org/10.13039/501100000320Alzheimer's Society: PG-2012-208. RS Macdonald Charitable Trust; Muir Maxwell Epilepsy Centre; Euan MacDonald Centre; Patrick Wild Centre; http://doi.org/10.13039/100005339American Academy of Neurology (AAN); http://doi.org/10.13039/501100000295Epilepsy Research UK (ERUK); http://doi.org/10.13039/501100000265Medical Research Council (MRC): MR/M024075/1.

Conflict of Interest: Authors declare no conflict of interest.

R.B., A.D.L., and A.G.-S. are contributed equally to this work.

Correspondence should be addressed to: Iris Oren, Centre for Discovery Brain Sciences, University of Edinburgh, 1 George Square, EH8 9JZ, UK. E-mail: iris.oren@ed.ac.uk

Cite as: eNeuro 2018; 10.1523/ENEURO.0426-17.2018

1. **Manuscript Title:** Circadian and brain state modulation of network hyperexcitability in Alzheimer's disease

2. **Abbreviated title:** Hyperexcitability modulation in AD

3. **Authors and affiliations:**

Rosalind Brown[1]*, Alice D. Lam[2,3]*, Alfredo Gonzalez-Sulser[1]*, Andrew Ying[1], Mary Jones[1], Robert C.-C. Chou[1], Makis Tzioras[1], Crispin Y. Jordan[1], Izabela Jedrasiak-Cape[1], Anne-Laure Hemonnot[4], Maurice Abou Jaoude[3], Andrew J. Cole[2,3], Sydney S. Cash[2,3], Takashi Saito[5], Takaomi Saido[5], Richard R. Ribchester[1], Kevan Hashemi[6], Iris Oren[1]

* These authors contributed equally to this work

1. Centre for Discovery Brain Sciences, University of Edinburgh, Edinburgh, UK
2. Epilepsy Division, Massachusetts General Hospital, Boston MA, USA
3. Harvard Medical School, Boston MA, USA
4. Université de Montpellier, Montpellier, France.
5. Laboratory for Proteolytic Neuroscience, RIKEN Brain Science Institute, Japan
6. OpenSource Instruments Inc., Watertown, MA, USA

4. **Author Contributions:**

RB, RRR and IO designed research

RB, ADL, AG-S, MJ, RC-CC, IJ-C, A-LH, TS and TS performed research

ADL, AY, RC-CC, MT, CYJ, A-LH and IO analysed the data

MAJ, AJC, SSC and KH contributed unpublished analytical tools

RB, ADL, KH and IO wrote the paper

5. **Correspondence should be addressed to:**

Iris Oren

Centre for Discovery Brain Sciences

University of Edinburgh

1 George Square

EH8 9JZ

UK

iris.oren@ed.ac.uk

6. **Number of Figures:** 7
7. **Number of Tables:** 2
8. **Number of Multimedia:** 0
9. **Number of words for Abstract:** 250
10. **Number of words for Significance Statement:** 111
11. **Number of words for Introduction:** 656
12. **Number of words for Discussion:** 2069
13. **Acknowledgements:** We thank the Gladstone Institute for providing J20 mice. We thank Dominic Walsh for supplying $APP^{NL/F}$ mice.
14. **Conflict of interest:** The authors declare no conflict of interest.
15. **Funding sources:** This work was supported by the grants awarded to IO from the following funders: the Alzheimer's Society (PG-2012-208), the RS Macdonald Charitable Trust, The Muir Maxwell Epilepsy Centre, The Euan MacDonald Centre and The Patrick Wild Centre. ADL was supported

by the American Academy of Neurology Institute. AGS was supported by Epilepsy Research UK. RC-CC was supported by an MRC grant (MR/M024075/1) awarded to RRR.

16.

Abstract

Network hyperexcitability is a feature of Alzheimer's disease (AD) as well as numerous transgenic mouse models of AD. While hyperexcitability in AD patients and AD animal models share certain features, the mechanistic overlap remains to be established. We aimed to identify features of network hyperexcitability in AD models that can be related to epileptiform activity signatures in AD patients. We studied network hyperexcitability in mice expressing amyloid precursor protein (APP) with mutations that cause familial AD, and compared a transgenic model that overexpresses human APP (J20), to a knock-in model expressing APP at physiological levels ($APP^{NL/F}$). We recorded continuous long-term electrocorticogram activity from mice, and studied modulation by circadian cycle, behavioural, and brain state. We report that while J20s exhibit frequent inter-ictal spikes (IIS), $APP^{NL/F}$ mice do not. In J20 mice, IIS were most prevalent during daylight hours and the circadian modulation was associated with sleep. Further analysis of brain state revealed that IIS in J20s are associated with features of rapid-eye movement (REM) sleep. We found no evidence of cholinergic changes that may contribute to IIS-circadian coupling in J20s. In contrast to J20s, intracranial recordings capturing IIS in AD patients demonstrated frequent IIS in non-REM sleep. The salient differences in sleep-stage coupling of IIS in APP overexpressing mice and AD patients suggests that different mechanisms may underlie network hyperexcitability in mice and humans. We posit that sleep-stage coupling of IIS should be an important consideration in identifying mouse AD models that most closely recapitulate

network hyperexcitability in human AD.

Significance statement

It is increasingly recognized that Alzheimer's disease (AD) is associated with hyperexcitability in brain networks. Brain network hyperexcitability is also reported in several rodent models of AD. We studied the signatures of this hyperexcitability in two rodent models of AD as well as AD patients. Network hyperexcitability was prevalent in a transgenic model of AD, but was absent in a rodent model that is considered to be more physiological. Moreover, while network hyperexcitability was coupled to rapid-eye movement (REM) sleep in transgenic mice, hyperexcitability occurred in non-REM sleep in AD patients. We suggest that brain state coupling of hyperexcitability can be used as a method for screening animal models of AD.

Introduction

An increased incidence of seizures in Alzheimer's disease (AD) is indicative of an underlying network hyperexcitability (Hesdorffer et al., 1996; Amatniek et al., 2006; Lozsadi and Larner, 2006; Vossel et al., 2013; Cretin et al., 2016). Inter-ictal spikes (IIS) are also seen in a high proportion of AD patients without a history of clinical seizures (Vossel et al., 2016). Non-ictal network hyperactivity has also been detected by means of fMRI in individuals at risk of developing dementia, for example in people carrying the APOE4 allele (Bookheimer et al., 2000; Filippini et al., 2009), with other genetic predictors of AD (Quiroz et al., 2010) and also in patients with mild cognitive impairment – a diagnosis which is considered to be a prodromal stage of AD (Dickerson et al., 2005). Network hyperexcitability and seizure activity appear at early stages of the disease and have been suggested to be predictors of accelerated cognitive decline (Amatniek et al., 2006; Vossel et al., 2013; Cretin et al., 2016; Vossel et al., 2016).

Network hyperexcitability has also been reported in numerous mouse models of AD pathology (Palop et al., 2007; Minkeviciene et al., 2009; Busche et al., 2012; Šišková et al., 2014; Kazim et al., 2017), with the aberrant activity being a feature that occurs in advance of plaque deposition (Busche et al., 2012; Bezzina et al., 2015). These phenomenological similarities have led to the suggestion that these animal models can provide a tool by which to study network hyperexcitability in human AD (Palop and Mucke, 2016).

Aberrant network activity could in itself contribute to neurodegeneration and cognitive dysfunction in AD pathology (Cirrito et al., 2005; Bero et al., 2011; Busche and Konnerth, 2015; Wu et al., 2016). Reducing network hyperexcitability has been shown to ameliorate cognitive dysfunction in both patients and animal models (Bakker et al., 2012; Sanchez et al., 2012; Haberman et al., 2017), and to attenuate Aβ pathology (Yuan and Grutzendler, 2016). Hence, targeting network hyperexcitability has been suggested as a novel therapeutic avenue for AD. However, studying this therapeutic avenue by means of animal models (Sanchez et al., 2012) requires a deeper understanding of the shared features of network hyperexcitability between AD patients and animal models.

Expression of epileptiform activity frequently exhibits a circadian pattern and shows preferential activation with specific brain states in a range of epilepsies (Quigg, 2000; Ng and Pavlova, 2013; Sedigh-Sarvestani et al., 2015). Circadian dysfunction and sleep disruption are common features of AD, and are also considered as early features of disease pathogenesis (Musiek et al., 2015; Mander et al., 2016; Musiek et al., 2018). Two recent papers have reported modulation of epileptiform activity by circadian cycle and brain state in transgenic AD models. Epileptiform activity was more prevalent in daylight conditions, and was suggested to occur primarily during REM sleep (Born et al., 2014; Kam et al., 2016). If epileptiform activity is modulated by circadian-cycles and/or brain state in AD patients, it is possible that this might contribute to the reported circadian alterations and sleep dysfunction. In line with this, it has recently been shown that inter-ictal activity in AD patients is highly prevalent during sleep (Vossel et al., 2016; Horváth et al., 2017; Lam et al., 2017). The

modulation of ictal related activity by brain state points to a distinguishing feature that could be used to (a) uncover distinct mechanisms underlying hyperexcitability, and (b) ascertain the translational utility of specific animal models in studying network hyperexcitability. To this end, the present study aimed to investigate circadian and brain state modulation of network hyperexcitability in two rodent models of AD of differing aetiology: one in which hAPP is overexpressed and one in which APP is expressed at endogenous levels. In order to shed light on the translational utility of rodent AD models for studying network hyperexcitability in human AD, we further examined sleep-stage modulation of epileptiform activity in two patients with AD, using recordings from intracranial electrodes placed directly adjacent to the hippocampus.

Methods

Animals and animal maintenance

All animal procedures were performed in accordance with the [Author University] animal welfare committee regulations and were performed under a UK Home Office project license.

Heterozygous mice expressing hAPP with the KM670/671NL (Swedish) and V717F (Indiana) mutations on a PDGFβ promoter (J20; Mucke et al., 2000) were bred by crossing J20 +/- males with C57Bl6J females. Experiments used J20+/- (n=21) and J20 -/- (n=8) wild-type (WT) littermate controls. The mean age of J20 animals was 5 months (range: 3.3 – 6.5 months).

Homozygous knock-in mice expressing APP KM670/671NL (Swedish) and APP I716F (Iberian) mutations ($APP^{NL/F}$; Saito et al., 2014) were back-crossed onto C57Bl6J strain for at least 3 generations and were >99.8% cogenic with C57Bl6J. Experiments used $APP^{NL/F}$ +/+ (n=20) and age-matched non-littermate C57Bl6J WT controls (n=15). Animals were either 8 months or 12 months of age.

Both male and female mice were used. Mice were kept on a 7h-19h light-dark cycle in standard, open cages. Mice were group-housed prior to surgery and were housed individually post-surgery and during telemetry data acquisition.

Surgery and data acquisition

A subdural intracranial electrocorticogram (ECoG) recording electrode was positioned in the cortex overlying the hippocampus (co-ordinates x: -2.25 y: -2.46). A reference electrode was implanted either in the skull of the contralateral hemisphere, or above the cerebellum. Electrodes were either bare wire, or skull screws. An EEG transmitter (A3028B, Open Source Instruments) was implanted on the back of the animal subcutaneously. Animals were left to recover for at least 24 hours after surgery before the commencement of telemetry data acquisition. Telemetric ECoG data was acquired for approximately 3 days from each animal. Recording was either carried out continuously between days 1 to day 3 after surgery, or day 1, followed by day 5 to day 6.

ECoG data was acquired using an Opensource Instruments data acquisition system at 512sps as previously described (Chang et al., 2011).

Video data was acquired using a Basler aca1300-60gm gigE camera sampling at 10fps, or a Logitech C270 HD webcam sampling at 5fps. Video was acquired during the daylight hours.

ECoG Data processing

The raw ECoG data was analysed using custom written Tcl and C processors. ECoG data was analysed in 8s intervals. For each interval we extracted measures of data loss, spike count, delta power (0.1-3.9 Hz) and theta power (4-12 Hz). We defined intervals in which data loss exceeded 20% of samples as "lossy" intervals. Intervals in which delta power exceeded $0.16mV^2$ were classified as artifacts. Lossy and artifact intervals were excluded.

Inter-ictal spikes (IIS) in rodent ECoG were detected as follows. Each 8-s interval of EEG was treated as a two-dimensional path. One dimension is voltage, which was normalized by dividing by the mean absolute step size of the voltage in the 8-s interval. The mean absolute step size is the sum of the absolute changes in voltage from one sample to the next, divided by the number of samples. For an 8-s interval, the number of samples would be 4096 and a typical mean absolute step size for mouse EEG is around 12 μV. The other dimension is time, which was normalized by dividing by the sample period. The spike-finder proceeds along this EEG path in steps. With each step, it moves to the nearest sample on the path ahead. Whenever the spike-finder steps past one or more samples, it classifies these samples as an aberration in the path. Solitary aberrations larger than 20 mean absolute step sizes are classified as IIS. A series of IIS in which single

spikes were separated by <78ms (40 samples) were treated as a burst event and counted as one IIS event within the 8s interval.

For each J20 animal, the false positive rate of IIS detection was determined by randomly hopping through 100 8s intervals identified by the processor as containing IIS, and scoring them as true or false positives. The animal was excluded from analysis if the false positive rate exceeded 10%. One animal was excluded from analysis on this basis. In the remaining animals, the false positive rate ranged from 0 – 6% (mean false positive rate: 1.9%).

We observed that lossy and artifactual intervals resulted from movement and external sources of interference. We could not exclude the possibility that these events are non-randomly distributed across the 24hr cycle. Non-random exclusion of intervals would impact the evaluation of coupling of IIS. We thus set a criterion: if >5% of all 8s intervals were excluded due loss or artifact, the animal was excluded from calculations of coupling of IIS to circadian cycles, sleep-wake, and θ/δ. Two J20 animals were excluded from data reported in Fig 2-4 on this basis (25% and 16% of 8s intervals excluded in these animals).

Video analysis

Video data was manually scored to classify periods as 'sleep' or 'wake'. Based on previous reports, sustained inactivity ≥40s was classified as 'sleep', while stationary periods <40s and periods of movement were classified as 'wake' (Pack et al., 2007). Postural shifts during sleep epochs did not break sleep epochs.

241 Immunohistochemistry and imaging

242 Animals were killed by transcardial perfusion with N-methyl-D-glucamine
243 (NMDG)-based saline solution (in mM: 92 NMDG, 2.5 KCl, 1.25 NaH_2PO_4, 20
244 HEPES, 30 $NaHCO_3$, 25 glucose, 10 $MgCl_2$, 0.5 $CaCl_2$, sucrose to adjust osmolarity
245 to 315-330mOsm). Brains were post-fixed with 4% paraformaldehyde for 24h
246 then washed and stored in PBS. Samples were put in 50% or 30% sucrose, PBS
247 solution and 50% OCT solution for 24h before cutting, then placed in the same
248 solution and cut using a freezing microtome.
249
250 50µm sections were stored in PBS at 4°C. Slices were presoaked with 5% rabbit
251 normal serum (RNS, Vector S-5000), 0.2% Triton X-100, PBS solution for 30min
252 at room temperature (RT), followed by incubation with 3% RNS, 0.2% Triton X-
253 100, anti-Choline Acetyltransferase (ChAT; 1:500, Millipore #AB144P, RRID:
254 AB_2079751), PBS solution for 48h at 4°C. The sections were washed 3 times
255 with PBS 0.2% Triton X-100 for 5min each and then incubated in 3% RNS, anti-
256 Goat biotinylated (1:200), Dapi (1:5000, Sigma D9542-1MG), PBS solution for 1h
257 at RT. After 3 PBS 0.2% Triton X-100 washings of 5min each, the sections were
258 incubated with ABC reagent (Vectastain PK-6105 kit) prepared half an hour
259 before using and stored in foil at 4°C containing 0.1% of A, 0.1% of B, 0.01%
260 Triton X-100, PBS for 1h at RT. After 6 PBS washings of 10min each, the sections
261 were put in 3 3'-diaminobenzidine (Sigma D5905-50TAB), 0.02% $CoCl_2$ (1%
262 wt/vol), 0,04% $(NH_4)_2Ni(SO_4)_2$ (1% wt/vol) dH_20 solution for 30min at 4°C over
263 agitation. Then stained by adding 1.2% of fresh 1% H_20_2 per slice for 10 to 20s
264 until the slice darkened. The slices were then transferred and washed in PBS, 6
265 times for 10min each, mounted on a slide and dried for 30min at 50°C then

finally covered with Mowiol Embedding Medium and coverslips. Slides were stored at RT.

Imaging was performed on a Zeiss AX10 microscope using StereoInvestigator Software with a 5x/0.16 (420630-9900) apochromat air objective. Quantification was performed using StereoInvestigator Software "Optical Fractioner Workflow" probe with the following settings. Thickness of 50µm was manually defined and regions were selected using a 1.25x/0.03 (420310-9900) apochromat air objective for low magnification and then counted with a 10x/0.45 (420640-9900) apochromat air objective for high magnification. The border between medial septum (MS) and diagonal band of Broca (DB) was defined as a line between the two major island of Caleja. The regions were separated using different lines. The counting frame used was a square of 75µm size and the grid was a square of 150µm size. The counter was blind to genotype.

Oral administration of Donepezil

Donepezil hydrochloride (Sigma Aldrich, D6821) was orally administered in a jelly. Mice were trained to voluntarily consume jelly following the protocol described by Zhang (2011). Mice were given placebo jelly or a jelly containing a Donepezil dose of 1.8mg/kg. For experiments studying the effects of Donepezil on acetylcholinesterase (AChE) activity, jelly was given at 8am daily. For experiments studying the effects of Donepezil on IIS, jelly was given daily at either 8am, or 8pm to assess interactions of AChE modulation and circadian cycle. Since there was no effect of AChE on IIS, results were pooled.

Acetylcholinestrase (AChE) assay

Quantitative measurements of AChE enzymic activity were made using a modified Ellman method (Ellman et al., 1961; Rosenfeld et al., 2001). Stock solutions were acetylthiocholine iodide, used as the enzymic substrate (ATH; 1.7 mg/ml in PBS, Sigma-Aldrich), 5,5'-dithio-bis(2-nitrobenzoic acid) (DTNB, 0.8 mg/ml in PBS, Sigma-Aldrich). Briefly, brains were rapidly dissected from either WT or J20 mice. Neocortex was isolated, weighed and then homogenised using a Pellet Pestle (Sigma, Z 359971) in 9 volumes of 0.1M sodium phosphate buffer (pH 7.4) (Patel et al., 2014). 5 µl of brain homogenate was aliquoted into each well of a 96 –well plate, volume made up to 200 µl with PBS. DTNB (50 µl from stock) was added, followed by 50 µl of ATH substrate from stock. Measurement of absorption at 450 nm began immediately (<2 hours from dissection) and was measured every 5 mins for up to 30 mins using a MRX microplate reader (Dynex Technologies, Chantilly, USA). Thiocholine production in the test wells was expressed in units of nmoles/minute, calibrated with reference to the absorbance change over a range of concentrations giving a linear response using glutathione as the DTNB reactant (Eyer et al., 2003). Neostigmine (10 µM, Sigma-Aldrich) was used to completely inhibit AChE activity and establish there was no baseline drift during the measurements.

Human scalp EEG and foramen ovale (FO) electrode recordings

Human scalp EEG and FO electrode recordings were performed at the Massachusetts General Hospital, as described in detail previously (Lam et al., 2017). Scalp EEG electrodes were placed using the International 10-20 system, with additional T1 and T2 electrodes.

Sleep staging in patient data was performed by a board-certified clinical neurophysiologist (ADL) based on visual analysis of the full scalp EEG data. While dedicated electrooculogram and electromyogram channels were not recorded for these studies, the frontopolar scalp EEG electrodes allowed assessment of eye movements, while the frontopolar, frontal, and temporal electrodes allowed assessment of myogenic activity. Scalp EEG data was reviewed in 30 second epochs in the longitudinal anterior-posterior bipolar montage, using the Python module *wonambi* (https://github.com/wonambi-python/wonambi). Each 30 second epoch was classified as awake, NREM1, NREM2, NREM3, or REM, based on the American Academy for Sleep Medicine's manual for sleep scoring.

Spike quantification in patient data was performed by a board-certified clinical neurophysiologist (ADL), using a custom-made GUI in Matlab (Mathworks, Natick, MA). The GUI displayed 15 second epochs of left and right sided FO data, in both bipolar and common reference montages (common reference = C2), along with the EKG trace to allow exclusion of EKG artifact. The reviewer could adjust amplitudes for each trace as needed. For the MCI patient analyzed, contact #3 from the left FO electrode did not record properly and was excluded from analysis. The reviewer marked all spikes in each epoch. Epochs were presented in consecutive order, but the reviewer was otherwise blinded to the sleep stage for each epoch during the review. Instantaneous spike rates were calculated by determining the total number of left FO and right FO spikes detected within all 30 second epochs of the recording (which corresponded to

the sleep staging epochs above), and converting these rates to spikes per hour. Average spike rates within each sleep stage were calculated by summing the total number of spikes that occurred during each sleep stage and dividing by the total number of hours the patient spent in each respective sleep stage in the recording.

Spectral analysis of the FO electrodes was performed in Matlab, using the freely available Chronux toolbox (Mitra and Bokil, 2007). Analysis was performed on the LFO1, LFO2, RFO1, and RFO2 channels, as these were the deepest contacts and thus least prone to noise or artifact. Channels were each normalized to zero-mean, unit-variance. Multi-taper spectrograms were calculated for each normalized channel, using the Chronux script *mtspecgramc* with the following parameters: frequency range: 1-20Hz, window: 30 seconds; step size: 30 seconds; time-bandwidth product: 3, tapers: 5. This provided a spectral resolution of 0.2Hz. An average spectrogram across all FO channels was then generated, and the average spectral powers within the δ band (0-4Hz) and θ band (4-12Hz) were then calculated.

Statistics

Statistical data analysis was performed using R (version 3.2.0) including the 'dplyr' (Wickham et al., n.d.) and ggplot2 (Wickham, 2009) packages.

Assumptions for parametric tests were tested using Q-Q plots and residual plots. Data transformations or non-parametric tests were used for two-group comparisons in which test assumptions were violated.

For evaluating the effects of the fixed effects of age and genotype on the proportion of intervals containing more than one spike in $APP^{NL/F}$ animals, the data first underwent a square-root transformation and then fit using a linear model:

$$\sqrt{IntervalProportion} \sim Age + Genotype + \xi$$

where ξ is the error term.

The time of IIS was treated as circular variable. Each interval in which 1 or more IIS were detected was considered an event. The time of each event was evaluated as a phase of a circadian cycle. Circular data was analysed using circular statistics by means of the 'circular' package (Agostinelli and Lund, 2013). Circular outliers were identified using 'CircOutlier' package (Rambli et al., 2016).

For tests entailing random variables, linear models were fit using 'lme4'(Bates et al., 2015). Significance was tested using a log-likelihood test comparing the full model to a null model without the factor of interest.

For evaluation of the relationship between spike count and θ/δ, we described each θ/δ value as a member of one of three levels: i) $\theta/\delta \leq 1$; ii) $1 < \theta/\delta \leq 2$, and iii) $\theta/\delta > 2$. We then modelled spike count (Poisson-distributed) as a function of levels of θ/δ, using the R package 'MCMCglmm' (Hadfield, 2010). It should be noted that due to poor properties of a single model fitted across all animals

(fitting animal as a random effect and θ/δ factor as a fixed effect), separate models were fitted to individual animals without including a random effect. Thus the data do not allow for inference about the population.

Event-triggered averages of IIS were evaluated by considering each interval in which an IIS was detected as an event. If no intervals within +- 80s around the event were excluded, then the 160s window was included in the calculation of the event-triggered averages, else the event was excluded from the averaging. An event-triggered average was also evaluated around 2000 randomly sampled points.

For comparing θ/δ in intervals with IIS to θ/δ in intervals preceding IIS, we considered only interval pairs where the preceding interval did not contain IIS and fit the model

$$\left(\theta/\delta\right)^{1/4} \sim Index + Subject + \xi$$

where Index was a factor labelling whether the interval contained IIS or the preceding interval and modelled as a fixed effect, and Subject was a random effect with a random intercept.

For comparison of ChAT+ cells between genotypes, the model used was:

$$EstimatedCount \sim Genotype + Region + Subject + \xi$$

where genotype and region were fixed effects and subject was a random effect with a random intercept.

To study the effect of genotype and treatment of the Thiocholine production rate, the data of Thiocholine production was log-transformed. The model used was

$$\log(ThiocholineRate) \sim GenotypeTreatment + RepeatID + \xi$$

where GenotypeTreatment was a fixed effect and RepeatID was a random effect with a random intercept. Post-hoc tests for the linear model were performed using package 'multcomp' with the Holm correction method (Hothorn et al., 2008). It should be noted that while the treatment levels of control and donepezil were independent, the neostigmine treatment was applied to a sample of wild-type control tissue and thus was not independent. This repeated factor was not accounted for in the model.

Significance was tested using α=0.05. Two-sided hypothesis testing was used.

Superscripts following statistical reporting in the results section refer to the statistical table (Table 1).

Code and data accessibility

The processor script used for quantification of IIS, θ and δ power in rodent ECoG data is available from http://www.opensourceinstruments.com/Electronics/A3018/HTML/SCPP4V1.tcl

Code used for quantifying IIS in human data is available from https://github.com/mauriceaj/GUI-EEG_Spike_Annotation

The datasets used for figures 1 – 6 (rodent data) are available from http://dx.doi.org/10.7488/ds/2319

Results

Network hyperexcitability in mouse models of AD pathology

To establish circadian patterns of network hyperexcitability in J20 mice, we recorded ECoG activity from freely-moving J20 and littermate wild-type (WT) mice using wireless telemetry over a period of three days. As network excitability has been suggested to be an early event in AD pathogenesis (Vossel et al., 2013; Sarkis et al., 2015), we focused our study on ages which precede overt plaque pathology in J20s (Mucke et al., 2000).

As previously reported (Palop et al., 2007), non-seizure, inter-ictal spikes (IIS; Fig 1A) were detected in J20 ECoG (note that while ictal activity was not assessed, we refer to these as inter-ictal events due to the similarity with IIS that have been reported in the literature) . We applied automated event detection (see methods), on 8s intervals of continuous ECoG. The percentage of intervals in which 1 or more spikes were detected was negligible in WTs (mean percentage: 0.8%, sd=0.7%, n=8). In contrast, the percentage of intervals with 1 or more spikes was greater in J20s (mean percentage: 11.6%, sd=5.1%, n=18; $t=10.6$, $df=23.98$, $p<0.0001$, t-test on square root transformed data with Welch correction, Figure 1B,C)[a].

Seizures and IIS have been reported in numerous strains of transgenic mice that express hAPP and that exhibit Aβ pathology (Del Vecchio et al., 2004; Palop et al.,

2007; Minkeviciene et al., 2009; Rasch and Born, 2013). However, it has been suggested that such network hyperexcitability is the result of overexpression of hAPP (Born et al., 2014). To determine whether network hyperexcitability is associated with Aβ pathology in the absence of hAPP overexpression, we performed telemetric ECoG recordings as above, in mice expressing the humanized Aβ sequence of APP ($APP^{NL/F}$; Saito et al., 2014) and age-matched controls. We recorded from mice at ages preceding overt plaque pathology (8 months) and at ages where plaques begin to appear (12 months)(Saito et al., 2014; Masuda et al., 2016). We found no significant effect of genotype in the proportion of intervals containing spikes between WT and $APP^{NL/F}$ (Fig 1D; $F(2, 32)=3.1$, $R^2=0.11$, $p=0.06$)[b] with a negligible proportion of intervals with one or more spikes detected (mean percentage of intervals with one or more spikes, pooled across genotype and age = 1.2%, 95%CI (0.8%, 1.6%)). A post-hoc power calculation based on the effect size from the J20 group (Cohen's d=2.5) and the sample sizes of the $APP^{NL/F}$ and WT groups yielded a power of >0.99 at $\alpha=0.05$ for an effect of genotype. Hence, we conclude that $APP^{NL/F}$ mice show no evidence of network hyperexcitability compared to control animals.

Circadian coupling of IIS

It has been suggested that seizure-related activity shows circadian fluctuations in epilepsies (Quigg, 2000). Hence we next asked whether the likelihood of IIS in J20s varies across the day/night cycle. Quantifying the number of IIS per hour revealed that IIS are more frequent during daylight hours (inactive phase; Fig 2A). We used circular statistics to extract measures of the phase coupling of IIS to the circadian cycle within individual J20 animals (Fig 2A, see methods). To

485 evaluate the degree of phase coupling of IIS in each animal, we evaluated the
486 mean angular vector length (ρ) from the time of IIS. ρ can vary between 0 (no
487 phase coupling) to 1 (perfect phase coupling). To evaluate the time to which IIS
488 were coupled, we extracted the mean coupling phase off IIS, expressed as a time
489 on a 24-hour cycle (φ_{IIS}).
490
491 The distribution of IIS phases differed significantly from a random distribution in
492 all animals (Rayleigh Test of Uniformity: $p<10^{-11}$). The extent of phase coupling
493 was variable across the sample of J20s (Fig 2B; mean ρ_{IIS}=0.24, sd=0.13, n=16).
494
495 Evaluating the coupling phase revealed that IIS occurred predominantly in the
496 light condition (Fig 2A). Across the sample of J20s, the mean φ_{IIS} ($\overline{\varphi_{IIS}}$)
497 confirmed this (Fig 2B; $\overline{\varphi_{IIS}}$ = 15h05, ρ =0.38, n=16, p < 0.0001, Rayleigh's test).
498 Inspection of the φ_{IIS} distribution revealed potential outliers. Testing for outliers
499 on a circular distribution (Rambli et al., 2016) identified four outliers. These four
500 animals were amongst the 5 that showed a cluster of weakest phase coupling as
501 measured by ρ_{IIS} (range: 0.06 – 0.11). We used the upper bound of the range of
502 ρ_{IIS} of the four outlier animals to classify phase-coupling as weak or strong.
503 Henceforth, we refer to the five animals with $\rho_{IIS} \leq 0.11$ as showing weak phase-
504 coupling, and the other 11 animals as showing strong phase-coupling (ρ_{IIS}>0.17).
505
506 <u>Sleep/wake modulation of IIS</u>
507 Since IIS predominantly occurred in the normal inactive phase of the circadian
508 cycle, we next asked whether this circadian modulation of IIS could be accounted

for by the sleep/wake state of the animals. In a subset of J20s, we acquired simultaneous video recordings while recording ECoG data (n=4). We manually scored the video and classified periods as 'sleep' or 'wake' (see Methods). Two of these four J20 animals showed strong circadian phase-coupling of IIS, and two showed weak phase-coupling. For the two animals that showed strong phase-coupling of IIS, IIS occurred more frequently in sleep than during waking (Fig 3A, B). In contrast, the modulation of IIS probability did not show a consistent pattern in animals showing weak phase-coupling (Fig 3B). This suggests that the strong phase-coupling of IIS may be accounted for by differences in behavioural state across the circadian cycle.

Brain state modulation of IIS in J20 mice

Sleep-related ictal and inter-ictal activity is differentially modulated by REM and NREM sleep in different forms of epilepsy (Bazil and Walczak, 1997; Herman et al., 2001; Sedigh-Sarvestani et al., 2014; Ewell et al., 2015). REM and NREM can be distinguished by the relative power in the δ (defined here as 0.1 – 3.9 Hz) and θ (4- 12 Hz) frequency bands, with high θ/δ associated with REM (Ewell et al., 2015) as well as waking exploration (Buzsáki, 2002). Thus, we next asked whether IIS are more likely to occur in particular brain states. To this end, we performed spectral analysis of the ECoG data from a subset of the mice (n=5 J20s) in which a reference electrode was implanted at cerebellar coordinates (a non-cortical reference for detection of cortical rhythms). ECoG recordings from J20 mice, exhibited periods showing a peak in θ-band power when animals were either awake (i.e. moving) or asleep, while periods of elevated δ-band power were seen during sleep (Fig 4A). We evaluated the θ/δ ratio for each 8s interval

and related it to the number of IIS in the interval. Transient increases in θ/δ were observed during sleep and were associated with increased occurrences of IIS (Fig 4B).

To quantify whether IIS were more likely in particular brain states, we next investigated the relationship between θ/δ and IIS count/8s interval. As we were interested in discriminating between REM and NREM sleep, we limited the analysis to daylight hours when animals are more likely to be asleep. We used a value of θ/δ<1 and >2 to classify periods as NREM-like and REM-like respectively (Ewell et al., 2015). This revealed significantly higher spike counts during REM-like vs NREM-like periods in all 5 animals (Fig 4B, $p<0.0005$ for all 5 animals, Markov Chain Monte Carlo generalised linear model)[c]. Interestingly, IIS were associated with increased θ/δ in animals showing both weak and strong phase-coupling (Fig 4C). Since sleep and wake are not predictive of IIS in animals with weak phase-coupling, this suggests that there is a mismatch between θ/δ and behavioural state in animals with weak phase-coupling. Moreover, high θ/δ states are predictive of IIS, regardless of behavioural state.

To examine the temporal dynamics of θ/δ around IIS, we evaluated the IIS-triggered average of θ/δ (Sedigh-Sarvestani et al., 2014) for 160s window around each interval in which at least one IIS was identified. In all animals, θ/δ was increased around the time of IIS relative to θ/δ averaged around randomly sampled points (Fig 4D). In three strongly phase-coupled animals, θ/δ returned to baseline levels within the 160s window around the event. However, in the

558 weakly phase coupled animals, θ/δ remained elevated above baseline levels in
559 this window. The peak in the θ/δ IIS-triggered average did not occur at t=0 in any
560 of the animals. Since intervals neighbouring the IIS-containing interval show
561 increased θ/δ, this suggests that the IIS contribution to spectral power did not
562 underlie the association between increases in θ/δ and IIS probability. To further
563 examine whether IIS could directly contribute to the increased θ/δ, we compared
564 θ/δ in intervals with IIS to θ/δ in the preceding intervals only in cases where the
565 preceding interval contained no IIS. We found no significant difference in
566 θ/δ between intervals with IIS and the preceding interval (Linear mixed model,
567 $\chi^2(1) = 0.35$, p=0.56, data not shown)[d].
568
569 To determine whether the spectral ECoG patterns in J20 mice are a reflection of
570 normal sleep or a result of pathology, we performed similar analysis of video-
571 scored ECoG data from 3 wild-type mice. As in the J20, intervals of strong
572 θ power were evident during wake and sleep, while periods of prominent
573 δ–band activity were seen in sleep. Transient increases in θ/δ during sleep akin
574 to those seen in J20s were also observed in all WT animals, suggesting that such
575 increases are a feature of normal sleep, and not pathological (Fig 5). To compare
576 the distribution of θ/δ during sleep between genotypes, we calculated the range
577 and 90th percentile of θ/δ while animals were asleep (using data for which we
578 had video-scoring). Group sizes were too small for statistical comparison but
579 suggested that θ/δ values spanned a narrower range in J20 mice than in WT mice
580 (J20 mean range=(0.02, 10.0), 90th percentile=2.4, SD(1.1), n=4; WT mean
581 range=(0.04, 19.3), 90th percentile =5.4, SD(1.4), n=3; data not shown).

582

583 No evidence of cholinergic changes in J20 mice

584 Cholinergic levels exhibit a circadian modulation (Hut and Van der Zee, 2011),
585 and high cholinergic tone is implicated in generating θ oscillatory states (Buzsáki,
586 2002). In addition, cholinergic dysfunction has been suggested to be a key
587 feature of AD pathogenesis (Craig et al., 2011). Recently, it has been suggested
588 that cholinergic alterations may contribute to network excitability in the Tg2576
589 model of AD (Kam et al., 2016). Hence, we hypothesized that cholinergic changes
590 might underlie the brain-state dependent modulation of IIS in the J20 mice. We
591 used immunohistochemistry to quantify the number of ChAT+ cells in the MS
592 and DB, and asked whether the number of ChAT+ cells differs between J20 (n=7)
593 and WT (n=5) mice. Fitting a linear mixed model to the data, we found no effect
594 of genotype on the estimated number of ChAT+ cells in the MS or DB (Fig 6A;
595 Linear mixed model, $\chi^2(1)=0.0002$, p=0.99)[e].

596

597 AChE activity is reduced in AD (García-Ayllón et al., 2011). We assayed
598 cholinergic function by measuring AChE activity. AChE activity was quantified by
599 estimating the rate of thiocholine production in neocortical brain homogenates
600 (see methods). There was no significant difference in the rate of thiocholine
601 production in brain homogenates prepared from WT and J20 mice (V=15, p=0.06,
602 n=5 WT/J20, Wilcoxon signed rank test, matched by day of assay, Fig 6B)[f]. We
603 also wanted to directly test the effect of modulation of ACh levels on IIS.
604 However, using oral administration of Donepezil at a dose previously suggested
605 to achieve clinically relevant drug plasma levels (Dong et al., 2009) was
606 ineffective at altering AChE activity in brain homogenates. In contrast, a positive

607 control treatment of direct application of neostigmine to brain homogenate led
608 to a significant reduction in AChE activity (Fig 6B; Linear mixed model:
609 $\chi^2(4)=75.3$, $p<0.0001$. Post-hoc using Tukey paired comparisons: $p<0.0001$ for
610 neostigmine vs. each of the treatment and genotypes. $p>0.05$ for all other group
611 comparisons)[g]. Two days of oral Donepezil administration at this dose did not
612 affect the IIS rate in J20 mice ($t(11)=0.8$, $p=0.43$, paired t-test, data not shown)[h].
613
614 Sleep stage modulation of IIS in human AD
615 The first intracranial recordings in humans with AD were recently reported and
616 demonstrated marked activation of mesial temporal lobe (mTL) IIS during sleep
617 compared to the awake state (Lam et al., 2017). We further analyzed the
618 combined scalp EEG and intracranial electrode recordings from these two
619 patients to better understand the relationship between sleep stage and mTL IIS
620 rate in AD patients. One patient with advanced AD did not achieve REM sleep but
621 showed mTL IIS preferentially during NREM sleep as opposed to waking states
622 (Table 2, Patient 1). The second patient was a 67-year-old woman with amnestic
623 mild cognitive impairment (aMCI), an early stage of AD that is thought to
624 correspond to the early stage of AD modelled in our young J20 mice. The data
625 from this patient was used to compare the frequency of IIS in wake, NREM and
626 REM states.
627
628 We analyzed 14.25 consecutive hours of combined scalp EEG and FO recordings
629 from the aMCI patient, which spanned from ~ 7PM on the first day of FO
630 recording (FOD1) to 9:15AM the following morning (FOD2). Further recordings
631 were not analyzed, as the patient was initiated on treatment with the

anticonvulsant levetiracetam on the afternoon on FOD2. Of note, the patient underwent implantation with FO electrodes on FOD1 from ~ 12:40PM – 1:50 PM and received sevoflurane, propofol and midazolam during the procedure. She was awake and answering questions appropriately by 2:15PM on FOD1.

We performed sleep staging of the recording using the full scalp EEG data, and measured mTL spike rates using the bilateral FO electrode data (Figure 7A,B). As described previously, we found that mTL spiking in the aMCI patient was largely activated during sleep. In contrast to what we found in the young J20 mice, mTL spiking in the aMCI patient occurred with highest frequency during NREM sleep stages, particularly during NREM3, and were lowest during REM sleep (Figure 7 and Table 2). mTL IIS rates during REM sleep were also markedly lower than during wakefulness (Table 2). We also calculated spectral power in the θ and δ bands, as well as the θ/δ ratio, in the FO electrodes across sleep states (Figure 7C-E). Increases in both θ and δ power were seen with deepening stages of NREM sleep, while a reduction was seen with REM sleep. In contrast to what we observed in the J20 mice, the θ/δ ratio was reduced during periods of highest spike frequency (Figure 7E).

Discussion

Network hyperexcitability is a feature of AD. Here we compared patterns of network hyperexcitability in two rodent models of AD, as well as in two AD patients, in order to reveal shared phenomenological features with the disease, We show that while J20, (hAPP overexpressing) mice exhibit frequent IIS as

657 previously reported, $APP^{NL/F}$ mice (that express APP at physiological levels) do
658 not show evidence of network hyperexcitability. Moreover, IIS in J20s occur
659 primarily during daylight hours, and this circadian fluctuation is accounted for
660 by an increased probability of IIS during sleep. Interestingly, we found that IIS in
661 J20 mice are modulated by brain state, with increased likelihood of IIS in brain
662 states with high θ/δ activity, a marker of REM sleep. In contrast, patients with AD
663 showed prevalent IIS during NREM sleep. Moreover, in the one AD patient who
664 exhibited REM sleep, IIS frequency was lowest in REM compared to other sleep
665 states.
666
667 Circadian dysfunction and network hyperexcitability in AD
668 Brain network hyperexcitability in the form of IIS and seizures has now been
669 reported in numerous models of AD pathology (reviewed in Scharfman, 2012;
670 Born, 2015). Our data, along with those reported by others (Born et al., 2014;
671 Kam et al., 2016) reveal that network hyperexcitability in animals models of AD
672 can be modulated by the circadian cycle. Circadian disturbances in AD include
673 sleep fragmentation, increased daytime somnolence, and sundowning, the
674 phenomenon in which neuropsychiatric symptoms are heightened late in the day
675 (Peter-Derex et al., 2015). Animal models of AD have also been reported to show
676 disturbances in the circadian cycle, some of which overlap with patterns of
677 circadian alterations seen in patients (Huitrón-Reséndiz et al., 2002; Vloeberghs
678 et al., 2004; Wisor et al., 2005; Jyoti et al., 2010; Sterniczuk et al., 2010; Duncan et
679 al., 2012; Roh et al., 2012). Our findings of circadian modulation of network
680 hyperexcitability in AD raise the question of whether IIS might causally
681 contribute to the alterations in circadian-coupled behaviour observed in AD.

682 Future work investigating the effects of anti-epileptic drugs on circadian
683 alterations in AD would go towards answering this.
684
685 Brain state modulation of network excitability

686 Here we report that IIS in J20 animals are modulated by θ/δ, with higher IIS rates
687 seen in states of high θ/δ during sleep. The spectral patterns of ECoG that we
688 report here are in line with previous reports in WT mice, that have shown
689 increases in cortical EEG θ power in REM sleep relative to wake and NREM
690 (Brankačk et al., 2010). We also report transient increases in θ/δ in sleep in both
691 WT and J20 mice. Since these increases in θ/δ occur in both WT and J20s, they
692 are likely to be indicative of REM sleep periods (Ewell et al., 2015). Given that
693 J20 animals with strong circadian phase-coupling show highest IIS rates during
694 sleep this suggests that IIS in these animals are associated with REM sleep.

695 An alternative explanation for the association between IIS and high θ/δ during
696 sleep may be that IIS occur during ectopic θ in sleep, in the absence of a
697 concomitant drop in muscle tonus. A phenomenon of ictal activity during ectopic
698 θ has been reported in a mouse model of Huntington's disease (Pignatelli et al.,
699 2012). Without simultaneous EMG recordings, the present data cannot
700 conclusively distinguish between REM states and ectopic θ. In the human data,
701 analysis of θ/δ ratios showed that these were lowest during periods of highest IIS
702 frequency. This argues against the idea of IIS coupled to ectopic θ in humans,
703 though a more definitive assessment will require data from more AD subjects as
704 well as healthy elderly controls.

Our finding of an association between IIS and high θ/δ is in line with recent reports that young Tg2576 model of AD as well as mice overexpressing WT-hAPP also demonstrate IIS predominantly during states of high θ which the authors suggest is indicative of REM sleep (Kam et al., 2016).

The findings that IIS in multiple mouse models of AD are most likely to occur in REM-like states begs the question of what makes REM a pro-ictal state in these models. Both REM sleep and the awake state share common features of high θ/δ activity and high cholinergic tone (Vazquez and Baghdoyan, 2001; Lee et al., 2005), yet IIS occur much less frequently in the awake state in these models. There are several potential explanations for this. Firing rates of hippocampal neurons increase during REM (Grosmark et al., 2012), which might contribute to the propensity to seize. In addition, systems that normally show distinct activity in REM sleep vs. waking and NREM sleep might contribute to the pro-ictal REM state in these models (Sedigh-Sarvestani et al., 2014; Ewell et al., 2015; Kam et al., 2016). Unlike cholinergic neurons, which increase their activity in both REM and waking, monoaminergic neurons in brainstem nuclei (including the locus coeruleus and the tuberomammillary nucleus) as well as the dorsal raphe nucleus of the hypothalamus, show differential activity between these brain states. These neurons are highly active in waking, exhibit low firing rates in NREM sleep, and are quiescent during REM sleep (Lee and Dan, 2012). It may be that brain state modulation of one or more of these systems is disrupted in these mouse AD models, and other forms of epilepsy which show REM-coupling (Sedigh-Sarvestani et al., 2014; Ewell et al., 2015).

The present study quantified cholinergic neurons in MS and DB. Cholinergic

neurons in laterodorsal tegmental and pedunculopontine tegmental nuclei of the pontomesencephalic tegmentum have been suggested to control REM onset (Van Dort et al., 2015). In the rat, these neurons have been shown to be active during both wake and REM, however, firing rates are higher in REM, and correlate with θ/δ (Boucetta et al., 2014). Thus, changes to these neurons are also potential candidates for mediating the pro-ictal nature of REM sleep in J20 mice.

Kam et al.,(2016) reported that MS-DB cholinergic neuron number was unchanged in young Tg2576 mice. However, they found evidence to support the notion that overactivity of cholinergic neurons might contribute to IIS by showing that antagonism of muscarinic receptors reduced IIS in these animals. Hence they concluded that IIS during REM might be the result of cholinergic hyperfunction. We did not find evidence for cholinergic changes in J20 mice as quantified by the number of cholinergic neurons in MS-DB, or AChE activity. If cholinergic activity is indeed unaltered in J20 mice, future experiments using muscarinic antagonism in J20 mice could be used to investigate whether atropine can act to reduce IIS by reducing overall neuronal excitability, rather than by reversing cholinergic hyperfunction.

Our assay of cholinergic function was based on measurements of AChE enzymic activity in brain homogenate. There was no significant difference between AChE levels in WT and J20, or with donepezil treatment. While it is possible that post-mortem degradation of AChE could have masked differences in AChE levels, the robust effect of neostigmine supports the conclusion that the tissue contained functional AChEs.

In a subset of our animals, IIS were weakly-coupled to the circadian cycle and the sleep-wake pattern, but were still modulated by θ/δ. This suggests that the relationship between θ/δ and behavioural state might be disturbed in these animals. It is possible that these animals also exhibited greater disturbances in other elements of the circadian-cycle, such as a circadian decoupling of sleep quantity/quality.

During both REM and NREM, hippocampal neurons have been shown to replay firing patterns that were experienced prior to sleep (Skaggs and McNaughton, 1996; Louie and Wilson, 2001), and such precisely timed sequences are likely to be involved in the memory facilitation role of sleep. IIS are thought to arise from depolarization and synchronous firing of neurons. This firing is followed by an inhibition and reduction of firing (Holmes and Lenck-Santini, 2006). Thus, IIS during sleep are likely to interfere with the coordinated replay of firing sequences, and consequently, would be expected to contribute to memory impairments. In support of this, it has recently been shown that reducing IIS by treatment with anti-epileptic drugs, rescues memory deficits in J20s (Sanchez et al., 2012).

Relationship between IIS and AD pathology in mouse models

Here we report that while IIS are prevalent in hAPP overexpressing mice, $APP^{NL/F}$ mice that exhibit Aβ pathology without APP overexpression, do not exhibit IIS at two ages preceding widespread plaque deposition (8 and 12 months). This finding is in line with other reports that it is overexpression of hAPP that is causal in generating network hyperexcitability in these animal

models (Born et al., 2014; Xu et al., 2015; Kam et al., 2016). An alternative explanation of the presence of IIS in J20 but not $APP^{NL/F}$ mice may be differences in the levels of Aβ between the two models. However, levels of soluble Aβ in 6 month old J20 and 12 month old $APP^{NL/F}$ are comparable, and levels of total Aβ are higher in $APP^{NL/F}$ (Shankar et al., 2009; Saito et al., 2014). Thus it is unlikely that higher levels of Aβ in the J20s are a cause of IIS in this model.

Interestingly, $APP^{NL/F}$ mice begin to exhibit cognitive deficits at 8 months of age (Masuda et al., 2016), which suggests that cognitive deficits at these ages are not the result of IIS, as has been suggested for J20s (Sanchez et al., 2012). Moreover, differences in the types of memory affected in J20 and $APP^{NL/F}$ at ages preceding overt plaque deposition have been reported. Specifically, 4 – 6 month old J20s show impairments in hippocampal dependent spatial memory (Sanchez et al., 2012). In contrast, in 8-month old $APP^{NL/F}$ mice, spatial memory as assayed by a place preference task is intact. However, place-avoidance memory, which is also dependent on amygdala-circuits (Wilensky et al., 2000), is impaired (Masuda et al., 2016). It may be that hippocampus dependent processes are susceptible to interference by IIS while the disturbances in the non-hippocampal circuits result from processes independent of IIS.

<u>Differential sleep-stage coupling between mouse models of AD and human AD</u>

Lam et al., (2017) recently used intracranial electrode recordings to detect mTL IIS in two AD patients without a history of epilepsy. Here, we report that in these patients, IIS were predominantly associated with NREM sleep (ie. low θ/δ). In the patient with aMCI, IIS occurred most frequently in N3 sleep and were least

798 frequent in REM, with a greater than 4.5-fold difference in spike rates between
799 N3 and REM. In the AD patient, frequent IIS were seen during NREM sleep,
800 though REM sleep was absent from this patient's brief recording, in line with
801 previous reports of REM deficits in AD (Vitiello et al., 1984). Our findings from
802 intracranial electrodes in AD patients are consistent with prior scalp EEG studies
803 by Vossel et al., (2016), who reported that epileptiform discharges are highly
804 prevalent in sleep stages >2 (although the authors did not differentiate between
805 REM and NREM sleep). Although the means of characterising sleep differed
806 between rodents and patients, combined, these results point to important
807 differences in sleep stage coupling of epileptiform activity between rodent AD
808 models and humans with AD and suggest that the specific mechanisms that
809 underlie hyperexcitability in AD may differ between certain mouse models and
810 humans.

811 Analysis of ictal and inter-ictal activity in epilepsy patients has led the view that
812 NREM sleep is a generally pro-ictal state, whereas REM sleep is an anti-ictal state
813 (Sammaritano et al., 1991; Herman et al., 2001; Minecan et al., 2002; Ng and
814 Pavlova, 2013). Many animal models of epilepsy have also shown that seizures
815 are more frequent in NREM and rarely occur in REM (Shouse et al., 2000) .
816 Interestingly, rodent models of the same type of epilepsy can still exhibit
817 differences in the sleep-stage coupling of epileptiform activity. For example, in
818 both the kindling as well as the pilocarpine models of temporal lobe epilepsy in
819 rats, IIS are most common during NREM sleep (Colom et al., 2006; Gelinas et al.,
820 2016). In contrast, rats with either the tetanus toxin or the low-dose kainate
821 models of temporal lobe epilepsy have seizures that occur most commonly

during REM sleep (Sedigh-Sarvestani et al., 2014; Ewell et al., 2015). Based on this, we hypothesize that different mouse models of AD may have specific mechanisms underlying their network hyperexcitability, which could be differentially expressed through sleep-stage coupling of IIS. We propose that sleep-stage coupling of IIS should be an important factor for identifying mouse AD models that more closely resemble the EEG signature of network hyperexcitability in human AD.

838 **Figures**

839 **Figure 1**: Inter-ictal spikes (IIS) are prevalent in J20 mice, but not in APP knock-
840 in mice. (A) ECoG trace recorded from a J20 mouse showing IIS. Inset is 250ms
841 expansion around IIS event marked by *. (B) Empirical cumulative distribution
842 frequency plots for individual animals quantifying the number of detected IIS in
843 8s intervals across 3 days of recording in WT and J20s. Colours represent
844 distributions for individual animals. (C) Plot showing the proportion of intervals
845 with one or more detected IIS in WT and J20. (D) Plot showing the proportion of
846 intervals with one or more detected IIS in WT and $APP^{NL/F}$ at 8 months and 12
847 months. Bars represent medians. Whiskers extend to 1.5 IQR. *** $p<0.001$.
848
849 **Figure 2:** Circadian modulation of IIS. (A) Circular histogram of IIS counts over
850 three days of recording in an individual J20 mouse plotted on 24hr cycle. Light
851 condition indicated by shading. For the animal shown, φ_{IIS}= 14h38 and ρ=0.43.
852 (B) Summary data for φ_{IIS} vs ρ for all animals, shown on circular plot. Solid
853 symbols are strongly-coupled animals. Weakly coupled animals are shown with
854 orange fill.
855
856 **Figure 3:** The probability of IIS is modulated by behavioural state in strongly
857 phase-coupled animals. (A) IIS count/8s interval versus time over 2 hours of
858 ECoG recording in a J20 mouse, with sleep and wake indicated by shading. (Bi)
859 Mean spike rate in sleep and wake condition for strongly and weakly phase
860 coupled animals. Error bars: 95% CI. (ii) Circular histograms for a strongly (left)
861 and weakly (right) phase coupled animals using conventions as in Fig 2A.
862

Figure 4: IIS occur during high θ/δ states. (A) 8s ECoG signals (left) and corresponding power spectra (right) during different behavioural states recorded from a J20 mouse. A single IIS is seen in the sleep high θ state (ii). (B) Time series of δ power, θ power, θ/δ and spike count per 8s intervals across 2 hours of ECoG recorded from the same J20 mouse as shown in A. Black/grey symbols indicate sleep/wake as classified by simultaneous video data. Red symbols and vertical dotted lines indicate the 8s intervals for which the ECoG signal is shown in panel A (C) Spike number per 8s interval as a function of θ/δ in 5 animals (represented by different colours and connected by lines). The increase spike count in intervals with high θ/δ was seen in animals with both strong (filled symbols) and weak (open symbols) circadian phase-coupling. *** $p<0.001$ (D) IIS-triggered averages of θ/δ for 5 individual animals (black) and windowed averages triggered around 2000 randomly sampled points (grey) show an increased θ/δ around IIS. Strong/weak coupling shown in filled/open symbols. Error bars in B and C represent 95% CI.

Figure 5. Transient increases in θ/δ are non-pathological features of sleep. (A) 8s ECoG signals (left) and corresponding power spectra (right) during different behavioural states recorded from a WT mouse. (B) Time series of δ power, θ power and θ/δ per 8s interval across 2 hours of ECoG recorded from same WT mouse as shown in A. Black/grey symbols indicate sleep/wake as classified by simultaneous video data. Red symbols and vertical dotted lines indicate the 8s intervals for which the ECoG signal is shown in panel A.

Figure 6: No evidence of cholinergic alterations in J20s. (A) Immunostained brain section showing ChAT+ cells in medial septum (MS) and diagonal band of Broca (DB). Lower panel shows zoomed in region of upper panel (left) and corresponding regions of a negative control stained section (right). Upper right: quantification of stereological estimates of ChAT+ cell count in MS and DB in WT and J20. (B) AChE activity was assayed by the rate of thiocholine production in brain homogenate from WT and J20 in control conditions and following oral administration of donepezil (DPZ). The AChE activity was compared to a positive control of direct application of neostigmine (10μM) to the brain homogenate. Experimental repeat groups are indicated by different colours and connected lines. *** $p<0.001$.

Figure 7: Sleep stage coupling of mesial temporal lobe (mTL) spiking in a human with aMCI, a suspected early stage of AD. (A) Hypnogram showing the patient's sleep architecture, spanning from ~ 7PM on FOD1 to 9:15AM on FOD2. (B) Bar plot showing instantaneous mTL lobe spike rates over the course of the recording. Bars are colored by sleep stage, with light green for Wake, light blue for NREM (includes NREM1, NREM2, and NREM3), and dark blue for REM. The patient had three brief subclinical seizures (SZ) from the left FO electrodes during this recording, the timing of which is depicted by red vertical bars. (C-E): Plots showing (C) δ power (0-4Hz), (D) θ power (4-12Hz), and (E) θ/δ ratio of bilateral mTL activity, based on FO electrodes recordings. Dots represent the spectral power for each non-overlapping 30 second window of the recording. Power is measured in arbitrary units.

912 **Table 1:** Statistical table

913

914 **Table 2**: Average mTL spike rates were evaluated from foramen ovale electrodes

915 and related to sleep stage as assayed by scalp EEG in two patients with AD.

916

917

918

919

920

921

922

923

924

925

References

Agostinelli C, Lund U (2013) R package "circular": Circular Statistics. Available at: https://r-forge.r-project.org/projects/circular.

Amatniek JC, Hauser WA, DelCastillo-Castaneda C, Jacobs DM, Marder K, Bell K, Albert M, Brandt J, Stern Y (2006) Incidence and predictors of seizures in patients with Alzheimer's disease. Epilepsia 47:867–872.

Bakker A, Krauss GL, Albert MS, Speck CL, Jones LR, Stark CE, Yassa MA, Bassett SS, Shelton AL, Gallagher M (2012) Reduction of Hippocampal Hyperactivity Improves Cognition in Amnestic Mild Cognitive Impairment. Neuron 74:467–474.

Bates D, Mächler M, Bolker B, Walker S (2015) Fitting linear mixed-effects models using lme4. J Stat Softw 67:1–48.

Bazil CW, Walczak TS (1997) Effects of Sleep and Sleep Stage on Epileptic and Nonepileptic Seizures. Epilepsia 38:56–62.

Bero AW, Yan P, Roh JH, Cirrito JR, Stewart FR, Raichle ME, Lee J-M, Holtzman DM (2011) Neuronal activity regulates the regional vulnerability to amyloid-[beta] deposition. Nat Neurosci 14:750–756.

Bezzina C, Verret L, Juan C, Remaud J, Halley H, Rampon C, Dahan L (2015) Early Onset of Hypersynchronous Network Activity and Expression of a Marker of Chronic Seizures in the Tg2576 Mouse Model of Alzheimer's Disease. PLOS ONE 10:e0119910.

Bookheimer SY, Strojwas MH, Cohen MS, Saunders AM, Pericak-Vance MA, Mazziotta JC, Small GW (2000) Patterns of Brain Activation in People at Risk for Alzheimer's Disease. N Engl J Med 343:450–456.

Born HA (2015) Seizures in Alzheimer's disease. Neuroscience 286:251–263.

Born HA, Kim J-Y, Savjani RR, Das P, Dabaghian YA, Guo Q, Yoo JW, Schuler DR, Cirrito JR, Zheng H, Golde TE, Noebels JL, Jankowsky JL (2014) Genetic Suppression of Transgenic APP Rescues Hypersynchronous Network Activity in a Mouse Model of Alzeimer's Disease. J Neurosci 34:3826–3840.

Boucetta S, Cissé Y, Mainville L, Morales M, Jones BE (2014) Discharge Profiles across the Sleep–Waking Cycle of Identified Cholinergic, GABAergic, and Glutamatergic Neurons in the Pontomesencephalic Tegmentum of the Rat. The Journal of Neuroscience 34:4708–4727.

Brankačk J, Kukushka VI, Vyssotski AL, Draguhn A (2010) EEG gamma frequency and sleep–wake scoring in mice: Comparing two types of supervised classifiers. Brain Res 1322:59–71.

Busche MA, Chen X, Henning HA, Reichwald J, Staufenbiel M, Sakmann B, Konnerth A (2012) Critical Role of Soluble Amyloid-B for Early Hippocampal

964 Hyperactivity in a Mouse Model of Alzheimer's Disease. Proc Natl Acad Sci U
965 S A.

966 Busche MA, Konnerth A (2015) Neuronal hyperactivity – A key defect in
967 Alzheimer's disease? BioEssays 37:624–632.

968 Buzsáki G (2002) Theta Oscillations in the Hippocampus. Neuron 33:325–340.

969 Chang P, Hashemi KS, Walker MC (2011) A novel telemetry system for recording
970 EEG in small animals. J Neurosci Methods 201:106–115.

971 Cirrito JR, Yamada KA, Finn MB, Sloviter RS, Bales KR, May PC, Schoepp DD, Paul
972 SM, Mennerick S, Holtzman DM (2005) Synaptic activity regulates interstitial
973 fluid amyloid-beta levels in vivo. Neuron 48:913–922.

974 Colom LV, García-Hernández A, Castañeda MT, Perez-Cordova MG, Garrido-
975 Sanabria ER (2006) Septo-Hippocampal Networks in Chronically Epileptic
976 Rats: Potential Antiepileptic Effects of Theta Rhythm Generation. J
977 Neurophysiol 95:3645–3653.

978 Craig LA, Hong NS, McDonald RJ (2011) Revisiting the cholinergic hypothesis in
979 the development of Alzheimer's disease. Neurosci Biobehav Rev 35:1397–
980 1409.

981 Cretin B, Sellal F, Philippi N, Bousiges O, Di Bitonto L, Martin-Hunyadi C, Blanc F
982 (2016) Epileptic Prodromal Alzheimer's Disease, a Retrospective Study of 13
983 New Cases: Expanding the Spectrum of Alzheimer's Disease to an Epileptic
984 Variant? J Alzheimers Dis 52:1125–1133.

985 Del Vecchio RA, Gold LH, Novick SJ, Wong G, Hyde LA (2004) Increased seizure
986 threshold and severity in young transgenic CRND8 mice. Neurosci Lett
987 367:164–167.

988 Dickerson BC, Salat DH, Greve DN, Chua EF, Rand-Giovannetti E, Rentz DM,
989 Bertram L, Mullin K, Tanzi RE, Blacker D, Albert MS, Sperling RA (2005)
990 Increased hippocampal activation in mild cognitive impairment compared to
991 normal aging and AD. Neurology 65:404–411.

992 Dong H, Yuede CM, Coughlan CA, Murphy KM, Csernansky JG (2009) Effects of
993 Donepezil on Amyloid-β and Synapse Density in the Tg2576 Mouse Model of
994 Alzheimer's Disease. Brain Res 1303:169–178.

995 Duncan MJ, Smith JT, Franklin KM, Beckett TL, Murphy MP, St Clair DK, Donohue
996 KD, Striz M, O'Hara BF (2012) Effects of aging and genotype on circadian
997 rhythms, sleep, and clock gene expression in APPxPS1 knock-in mice, a
998 model for Alzheimer's disease. Exp Neurol 236:249–258.

999 Ellman GL, Courtney KD, Andres V, Feather-stone RM (1961) A new and rapid
1000 colorimetric determination of acetylcholinesterase activity. Biochem
1001 Pharmacol 7:88–95.

1002 Ewell LA, Liang L, Armstrong C, Soltesz I, Leutgeb S, Leutgeb JK (2015) Brain
1003 State Is a Major Factor in Preseizure Hippocampal Network Activity and
1004 Influences Success of Seizure Intervention. J Neurosci 35:15635–15648.

1005 Eyer P, Worek F, Kiderlen D, Sinko G, Stuglin A, Simeon-Rudolf V, Reiner E (2003)
1006 Molar absorption coefficients for the reduced Ellman reagent: reassessment.
1007 Anal Biochem 312:224–227.

1008 Filippini N, MacIntosh BJ, Hough MG, Goodwin GM, Frisoni GB, Smith SM,
1009 Matthews PM, Beckmann CF, Mackay CE (2009) Distinct Patterns of Brain
1010 Activity in Young Carriers of the APOE-E4 Allele. Proc Natl Acad Sci U S A
1011 106:7209–7214.

1012 García-Ayllón M-S, Small DH, Avila J, Sáez-Valero J (2011) Revisiting the Role of
1013 Acetylcholinesterase in Alzheimer's Disease: Cross-Talk with P-tau and β-
1014 Amyloid. Front Mol Neurosci 4:22.

1015 Gelinas J, Khodagholy D, Thesen T, Devinsky O, Buzsáki G (2016) Interictal
1016 epileptiform discharges induce hippocampal-cortical coupling in temporal
1017 lobe epilepsy. Nat Med 22:641–648.

1018 Grosmark AD, Mizuseki K, Pastalkova E, Diba K, Buzsáki G (2012) REM Sleep
1019 Reorganizes Hippocampal Excitability. Neuron 75:1001–1007.

1020 Haberman RP, Branch A, Gallagher M (2017) Targeting Neural Hyperactivity as a
1021 Treatment to Stem Progression of Late-Onset Alzheimer's Disease.
1022 Neurotherapeutics 14:662–676.

1023 Hadfield JD (2010) MCMC methods for multi-response generalized linear mixed
1024 models: the MCMCglmm. R package. J Stat Softw 33.

1025 Herman ST, Walczak TS, Bazil CW (2001) Distribution of partial seizures during
1026 the sleep--wake cycle: differences by seizure onset site. Neurology 56:1453–
1027 1459.

1028 Hesdorffer DC, Hauser WA, Annegers JF, Kokmen E, Rocca WA (1996) Dementia
1029 and adult-onset unprovoked seizures. Neurology 46:727–730.

1030 Holmes GL, Lenck-Santini P-P (2006) Role of interictal epileptiform
1031 abnormalities in cognitive impairment. Epilepsy Behav 8:504–515.

1032 Horváth A, Szűcs A, Barcs G, Kamondi A (2017) Sleep EEG Detects Epileptiform
1033 Activity in Alzheimer's Disease with High Sensitivity. J Alzheimers Dis
1034 56:1175–1183.

1035 Hothorn T, Bretz F, Westfall P (2008) Simultaneous inference in general
1036 parametric models. Biom J 50:346–363.

1037 Huitrón-Reséndiz S, Sánchez-Alavez M, Gallegos R, Berg G, Crawford E, Giacchino
1038 JL, Games D, Henriksen SJ, Criado JR (2002) Age-independent and age-
1039 related deficits in visuospatial learning, sleep–wake states, thermoregulation

1040 and motor activity in PDAPP mice. Brain Res 928:126–137.

1041 Hut RA, Van der Zee EA (2011) The cholinergic system, circadian rhythmicity,
1042 and time memory. Behav Brain Res 221:466–480.

1043 Jyoti A, Plano A, Riedel G, Platt B (2010) EEG, activity, and sleep architecture in a
1044 transgenic AβPPswe/PSEN1A246E Alzheimer's disease mouse. J Alzheimers
1045 Dis 22:873–887.

1046 Kam K, Duffy ÁM, Moretto J, LaFrancois JJ, Scharfman HE (2016) Interictal spikes
1047 during sleep are an early defect in the Tg2576 mouse model of β-amyloid
1048 neuropathology. Sci Rep 6:20119.

1049 Kazim SF, Chuang S-C, Zhao W, Wong RKS, Bianchi R, Iqbal K (2017) Early-Onset
1050 Network Hyperexcitability in Presymptomatic Alzheimer's Disease
1051 Transgenic Mice Is Suppressed by Passive Immunization with Anti-Human
1052 APP/Aβ Antibody and by mGluR5 Blockade. Front Aging Neurosci 9:1246.

1053 Lam AD, Deck G, Goldman A, Eskandar EN, Noebels J, Cole AJ (2017) Silent
1054 hippocampal seizures and spikes identified by foramen ovale electrodes in
1055 Alzheimer's disease. Nat Med 23:678–680.

1056 Lee MG, Hassani OK, Alonso A, Jones BE (2005) Cholinergic Basal Forebrain
1057 Neurons Burst with Theta during Waking and Paradoxical Sleep. J Neurosci
1058 25:4365–4369.

1059 Lee S-H, Dan Y (2012) Neuromodulation of Brain States. Neuron 76:209–222.

1060 Louie K, Wilson MA (2001) Temporally Structured Replay of Awake
1061 Hippocampal Ensemble Activity during Rapid Eye Movement Sleep. Neuron
1062 29:145–156.

1063 Lozsadi DA, Larner AJ (2006) Prevalence and causes of seizures at the time of
1064 diagnosis of probable Alzheimer's disease. Dement Geriatr Cogn Disord
1065 22:121–124.

1066 Mander BA, Winer JR, Jagust WJ, Walker MP (2016) Sleep: A Novel Mechanistic
1067 Pathway, Biomarker, and Treatment Target in the Pathology of Alzheimer's
1068 Disease? TINS 39:552–566.

1069 Masuda A, Kobayashi Y, Kogo N, Saito T, Saido TC, Itohara S (2016) Cognitive
1070 deficits in single App knock-in mouse models. Neurobiol Learn Mem 135:73–
1071 82.

1072 Minecan D, Natarajan A, Marzec M, Malow B (2002) Relationship of epileptic
1073 seizures to sleep stage and sleep depth. Sleep 25:899–904.

1074 Minkeviciene R, Rheims S, Dobszay MB, Zilberter M, Hartikainen J, Fulop L, Penke
1075 B, Zilberter Y, Harkany T, Pitkänen A, Tanila H (2009) Amyloid beta-Induced
1076 Neuronal Hyperexcitability Triggers Progressive Epilepsy. J Neurosci
1077 29:3453–3462.

1078 Mitra P, Bokil H (2007) Observed brain dynamics. Oxford University Press.

1079 Mucke L, Masliah E, Yu G-Q, Mallory M, Rockenstein EM, Tatsuno G, Hu K,
1080 Kholodenko D, Johnson-Wood K, McConlogue L (2000) High-Level Neuronal
1081 Expression of Aβ1–42 in Wild-Type Human Amyloid Protein Precursor
1082 Transgenic Mice: Synaptotoxicity without Plaque Formation. J Neurosci
1083 20:4050–4058.

1084 Musiek ES, Bhimasani M, Zangrilli MA, Morris JC, Holtzman DM, Ju Y-ES (2018)
1085 Circadian Rest-Activity Pattern Changes in Aging and Preclinical Alzheimer
1086 Disease. JAMA Neurol.

1087 Musiek ES, Xiong DD, Holtzman DM (2015) Sleep, circadian rhythms, and the
1088 pathogenesis of Alzheimer Disease. Exp Mol Med 47:e148.

1089 Ng M, Pavlova M (2013) Why Are Seizures Rare in Rapid Eye Movement Sleep?
1090 Review of the Frequency of Seizures in Different Sleep Stages. Epilepsy Res
1091 Treat 2013:1–10.

1092 Pack AI, Galante RJ, Maislin G, Cater J, Metaxas D, Lu S, Zhang L, Smith Von R, Kay
1093 T, Lian J, Svenson K, Peters LL (2007) Novel method for high-throughput
1094 phenotyping of sleep in mice. Physiol Genomics 28:232–238.

1095 Palop JJ, Chin J, Roberson ED, Wang J, Thwin MT, Bien-Ly N, Yoo J, Ho KO, Yu G-Q,
1096 Kreitzer A, Finkbeiner S, Noebels JL, Mucke L (2007) Aberrant Excitatory
1097 Neuronal Activity and Compensatory Remodeling of Inhibitory Hippocampal
1098 Circuits in Mouse Models of Alzheimer's Disease. Neuron 55:697–711.

1099 Palop JJ, Mucke L (2016) Network abnormalities and interneuron dysfunction in
1100 Alzheimer disease. Nat Rev Neurosci 17:777–792.

1101 Patel V, Oh A, Voit A, Sultatos LG, Babu GJ, Wilson BA, Ho M, McArdle JJ (2014)
1102 Altered Active Zones, Vesicle Pools, Nerve Terminal Conductivity, and
1103 Morphology during Experimental MuSK Myasthenia Gravis Phillips W, ed.
1104 PLOS ONE 9:e110571.

1105 Peter-Derex L, Yammine P, Bastuji H, Croisile B (2015) Sleep and Alzheimer's
1106 disease. Sleep Med Rev 19:29–38.

1107 Pignatelli M, Lebreton F, Cho YH, Leinekugel X (2012) “Ectopic” theta oscillations
1108 and interictal activity during slow-wave state in the R6/1 mouse model of
1109 Huntington's disease. Neurobiol Dis 48:409–417.

1110 Quigg M (2000) Circadian rhythms: interactions with seizures and epilepsy.
1111 Epilepsy Res.

1112 Quiroz YT, Budson AE, Celone K, Ruiz A, Newmark R, Castrillón G, Lopera F, Stern
1113 CE (2010) Hippocampal hyperactivation in presymptomatic familial
1114 Alzheimer's disease. Ann Neurol 68:865–875.

1115 Rambli A, Abuzaid AHM, Bin Mohamed I, Hussin AG (2016) Procedure for

1116 Detecting Outliers in a Circular Regression Model. PLOS ONE 11:e0153074.

1117 Rasch B, Born J (2013) About Sleep's Role in Memory. Physiol Rev 93:681–766.

1118 Roh JH, Huang Y, Bero AW, Kasten T, Stewart FR, Bateman RJ, Holtzman DM
1119 (2012) Disruption of the Sleep-Wake Cycle and Diurnal Fluctuation of β-
1120 Amyloid in Mice with Alzheimer's Disease Pathology. Sci Transl Med
1121 4:150ra122–150ra122.

1122 Rosenfeld C, Kousba A, Sultatos LG (2001) Interactions of rat brain
1123 acetylcholinesterase with the detergent Triton X-100 and the
1124 organophosphate paraoxon. Toxicol Sci 63:208–213.

1125 Saito T, Matsuba Y, Mihira N, Takano J, Nilsson P, Itohara S, Iwata N, Saido TC
1126 (2014) Single App knock-in mouse models of Alzheimer's disease. Nat
1127 Neurosci 17:661–663.

1128 Sammaritano M, Gigli GL, Gotman J (1991) Interictal spiking during wakefulness
1129 and sleep and the localization of foci in temporal lobe epilepsy. Neurology
1130 41:290–297.

1131 Sanchez PE, Zhu L, Verret L, Vossel KA, Orr AG, Cirrito JR, Devidze N, Ho K, Yu G-
1132 Q, Palop JJ, Mucke L (2012) Levetiracetam suppresses neuronal network
1133 dysfunction and reverses synaptic and cognitive deficits in an Alzheimer's
1134 disease model. Proc Natl Acad Sci U S A 109:E2895–E2903.

1135 Sarkis RA, Dickerson BC, Cole AJ, Chemali ZN (2015) Clinical and
1136 Neurophysiologic Characteristics of Unprovoked Seizures in Patients
1137 Diagnosed With Dementia. J Neuropsychiatry Clin Neurosci 28:56–61.

1138 Scharfman HE (2012) Alzheimer's disease and epilepsy: insight from animal
1139 models. Future Neurol 7:177–192.

1140 Sedigh-Sarvestani M, Blumenfeld H, Loddenkemper T, Bateman LM (2015)
1141 Seizures and brain regulatory systems: Consciousness, sleep, and autonomic
1142 systems. J Clin Neurophysiol 32:188–193.

1143 Sedigh-Sarvestani M, Thuku GI, Sunderam S, Parkar A, Weinstein SL, Schiff SJ,
1144 Gluckman BJ (2014) Rapid eye movement sleep and hippocampal theta
1145 oscillations precede seizure onset in the tetanus toxin model of temporal
1146 lobe epilepsy. J Neurosci 34:1105–1114.

1147 Shankar GM, Leissring MA, Adame A, Sun X, Spooner E, Masliah E, Selkoe DJ,
1148 Lemere CA, Walsh DM (2009) Biochemical and immunohistochemical
1149 analysis of an Alzheimer's disease mouse model reveals the presence of
1150 multiple cerebral Aβ assembly forms throughout life. Neurobiol Dis36:293–
1151 302.

1152 Shouse MN, Farber PR, Staba RJ (2000) Physiological basis: how NREM sleep
1153 components can promote and REM sleep components can suppress seizure
1154 discharge propagation. Clin Neurophysiol 111:S9–S18.

1155 Skaggs WE, McNaughton BL (1996) Replay of Neuronal Firing Sequences in Rat
1156 Hippocampus During Sleep Following Spatial Experience. Science 271:1870–
1157 1873.

1158 Sterniczuk R, Dyck RH, LaFerla FM, Antle MC (2010) Characterization of the
1159 3xTg-AD mouse model of Alzheimer's disease: part 1. Circadian changes.
1160 Brain Res 1348:139–148.

1161 Šišková Z, Justus D, Kaneko H, Friedrichs D, Henneberg N, Beutel T, Pitsch J,
1162 Schoch S, Becker A, Kammer von der H, Remy S (2014) Dendritic Structural
1163 Degeneration Is Functionally Linked to Cellular Hyperexcitability in a Mouse
1164 Model of Alzheimer's Disease. Neuron 84:1023–1033.

1165 Van Dort CJ, Zachs DP, Kenny JD, Zheng S, Goldblum RR, Gelwan NA, Ramos DM,
1166 Nolan MA, Wang K, Weng F-J, Lin Y, Wilson MA, Brown EN (2015)
1167 Optogenetic activation of cholinergic neurons in the PPT or LDT induces
1168 REM sleep. Proc Natl Acad Sci U S A112:584–589.

1169 Vazquez J, Baghdoyan HA (2001) Basal forebrain acetylcholine release during
1170 REM sleep is significantly greater than during waking. Am J Physiol
1171 280:R598–R601.

1172 Vitiello MV, Bokan JA, Kukull WA, Muniz RL, Smallwood RG, Prinz PN (1984)
1173 Rapid eye movement sleep measures of Alzheimer's-type dementia patients
1174 and optimally healthy aged individuals. Biol Psychiatry 19:721–734.

1175 Vloeberghs E, Van Dam D, Engelborghs S, Nagels G, Staufenbiel M, De Deyn PP
1176 (2004) Altered circadian locomotor activity in APP23 mice: a model for BPSD
1177 disturbances. Eur J Neurosci 20:2757–2766.

1178 Vossel KA, Beagle AJ, Rabinovici GD, Mucke L (2013) Seizures and epileptiform
1179 activity in the early stages of alzheimer disease. JAMA Neurol 70:1158–1166.

1180 Vossel KA, Ranasinghe KG, Beagle AJ, Mizuiri D, Honma SM, Dowling AF, Darwish
1181 SM, Van Berlo V, Barnes DE, Mantle M, Karydas AM, Coppola G, Roberson ED,
1182 Miller BL, Garcia PA, Kirsch HE, Mucke L, Nagarajan SS (2016) Incidence and
1183 impact of subclinical epileptiform activity in Alzheimer's disease. Ann Neurol
1184 80:858–870.

1185 Wickham H (2009) ggplot2: elegant graphics for data analysis. R package.

1186 Wickham H, Francois R (2015) dplyr: A grammar of data manipulation. R
1187 package

1188 Wilensky AE, Schafe GE, LeDoux JE (2000) The amygdala modulates memory
1189 consolidation of fear-motivated inhibitory avoidance learning but not
1190 classical fear conditioning. J Neurosci 20:7059–7066.

1191 Wisor JP, Edgar DM, Yesavage J, Ryan HS, McCormick CM, Lapustea N, Murphy
1192 GM (2005) Sleep and circadian abnormalities in a transgenic mouse model of
1193 Alzheimer's disease: a role for cholinergic transmission. Neuroscience

131:375–385.

Wu JW, Hussaini SA, Bastille IM, Rodriguez GA, Mrejeru A, Rilett K, Sanders DW, Cook C, Fu H, Boonen RACM, Herman M, Nahmani E, Emrani S, Figueroa YH, Diamond MI, Clelland CL, Wray S, Duff KE (2016) Neuronal activity enhances tau propagation and tau pathology in vivo. Nat Neurosci 19:1085–1092.

Xu W, Fitzgerald S, Nixon RA, Levy E, Wilson DA (2015) Early hyperactivity in lateral entorhinal cortex is associated with elevated levels of AβPP metabolites in the Tg2576 mouse model of Alzheimer's disease. Exp Neurol 264:82–91.

Yuan P, Grutzendler J (2016) Attenuation of -Amyloid Deposition and Neurotoxicity by Chemogenetic Modulation of Neural Activity. J Neurosci 36:632–641.

Zhang L (2011) Voluntary oral administration of drugs in mice. Protocol Exchange.

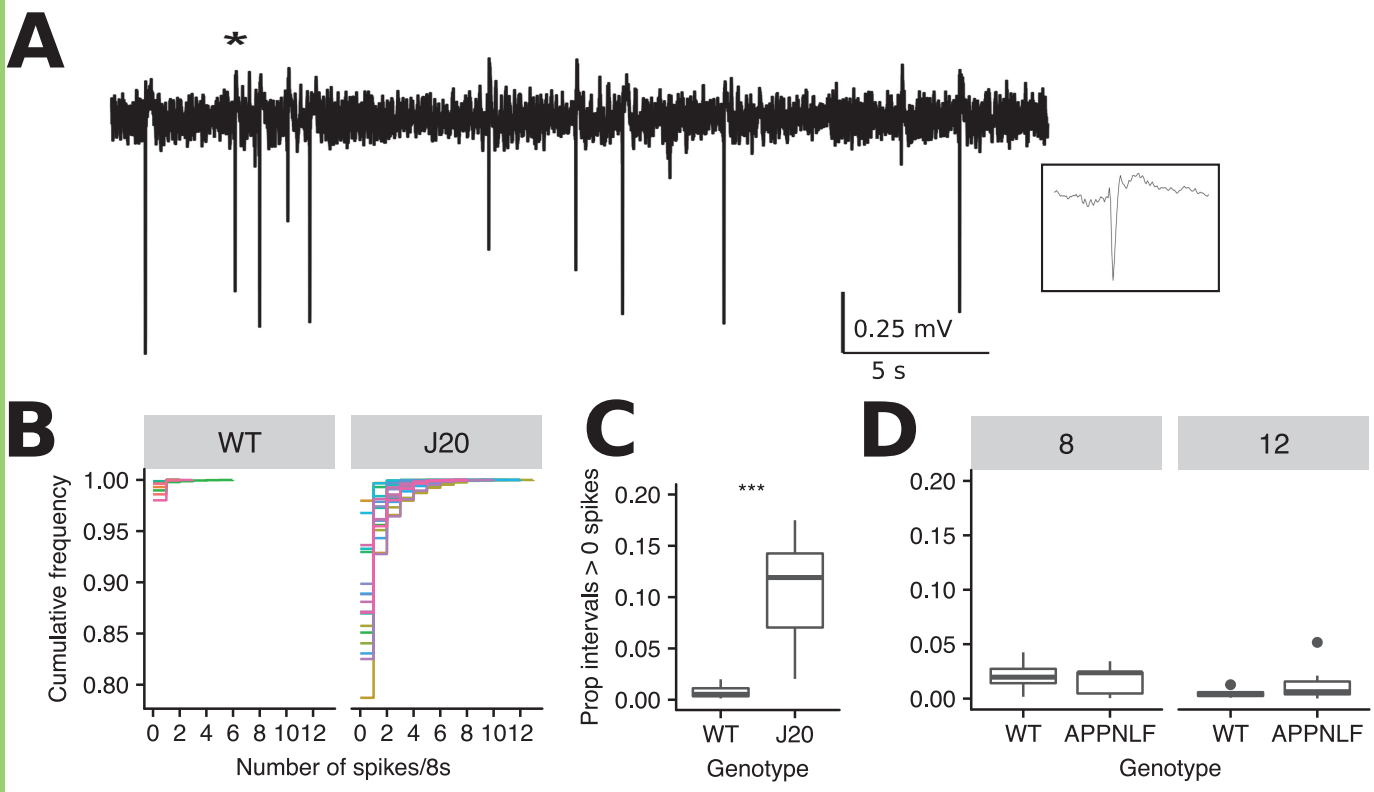

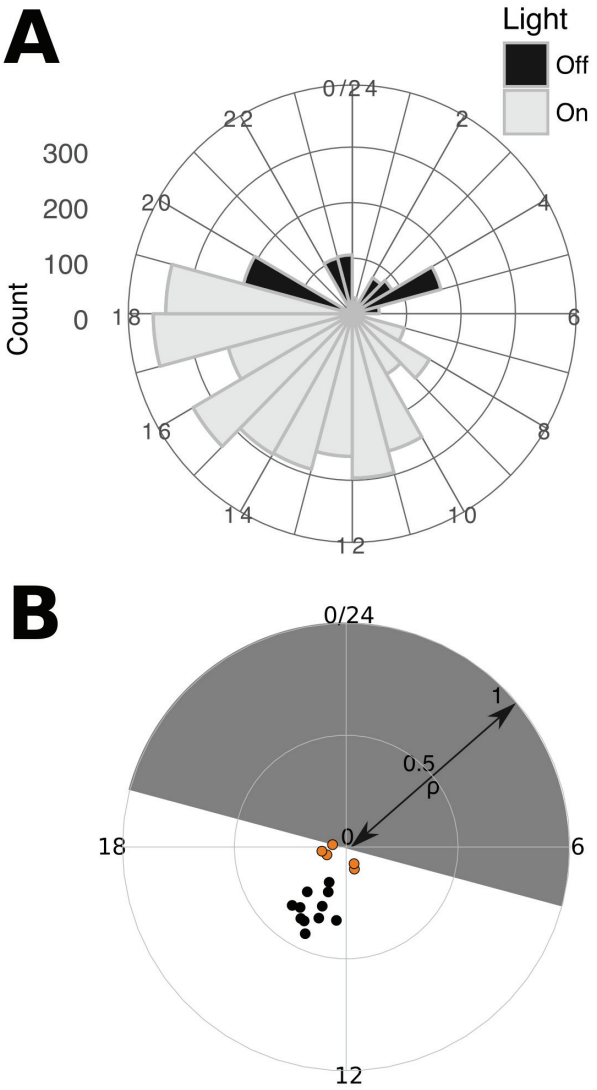

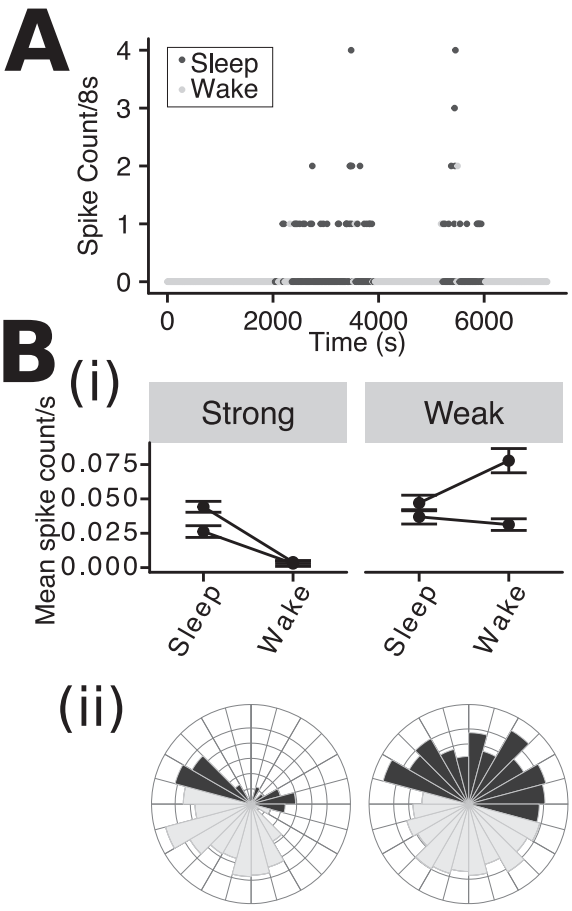

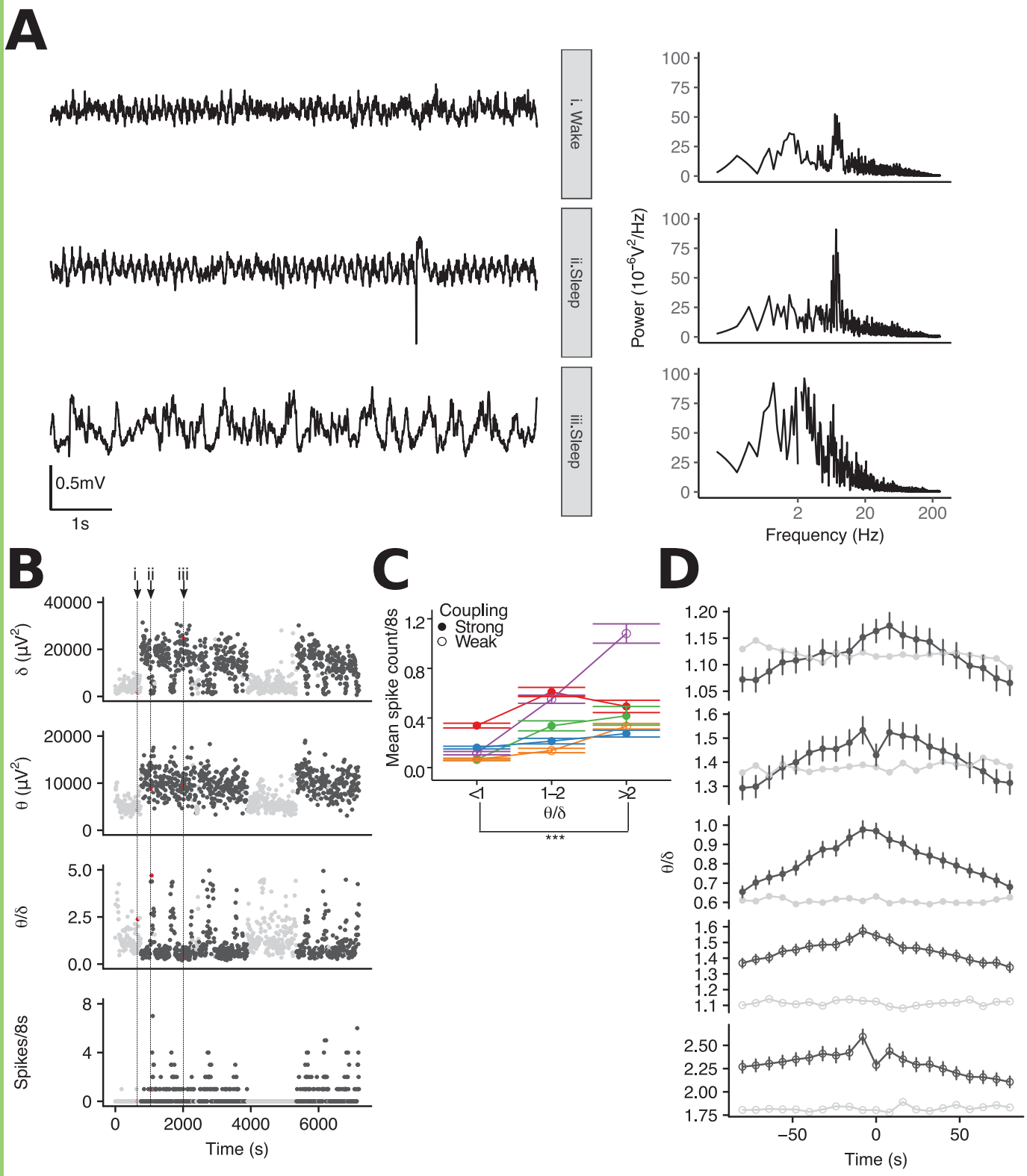

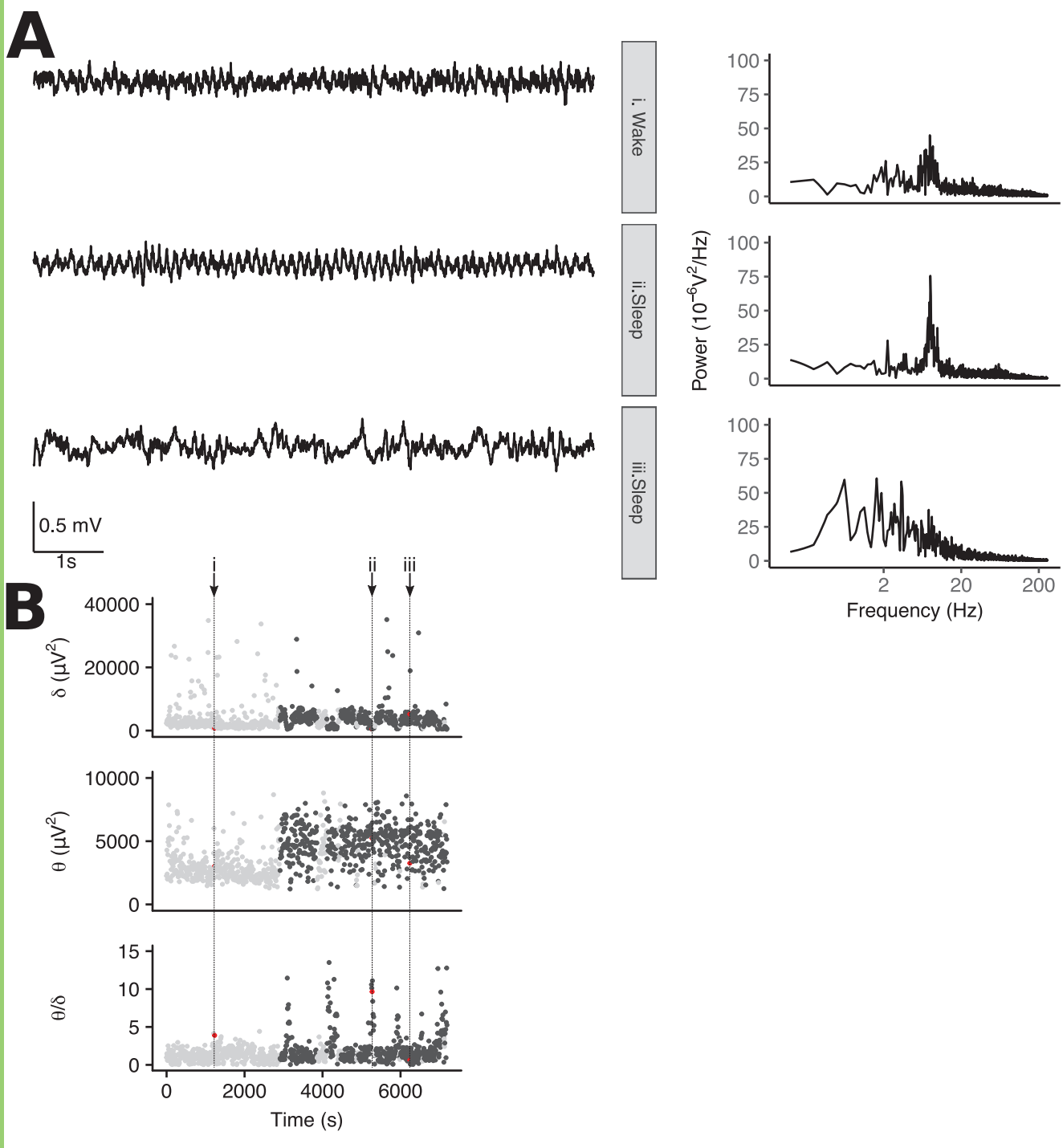

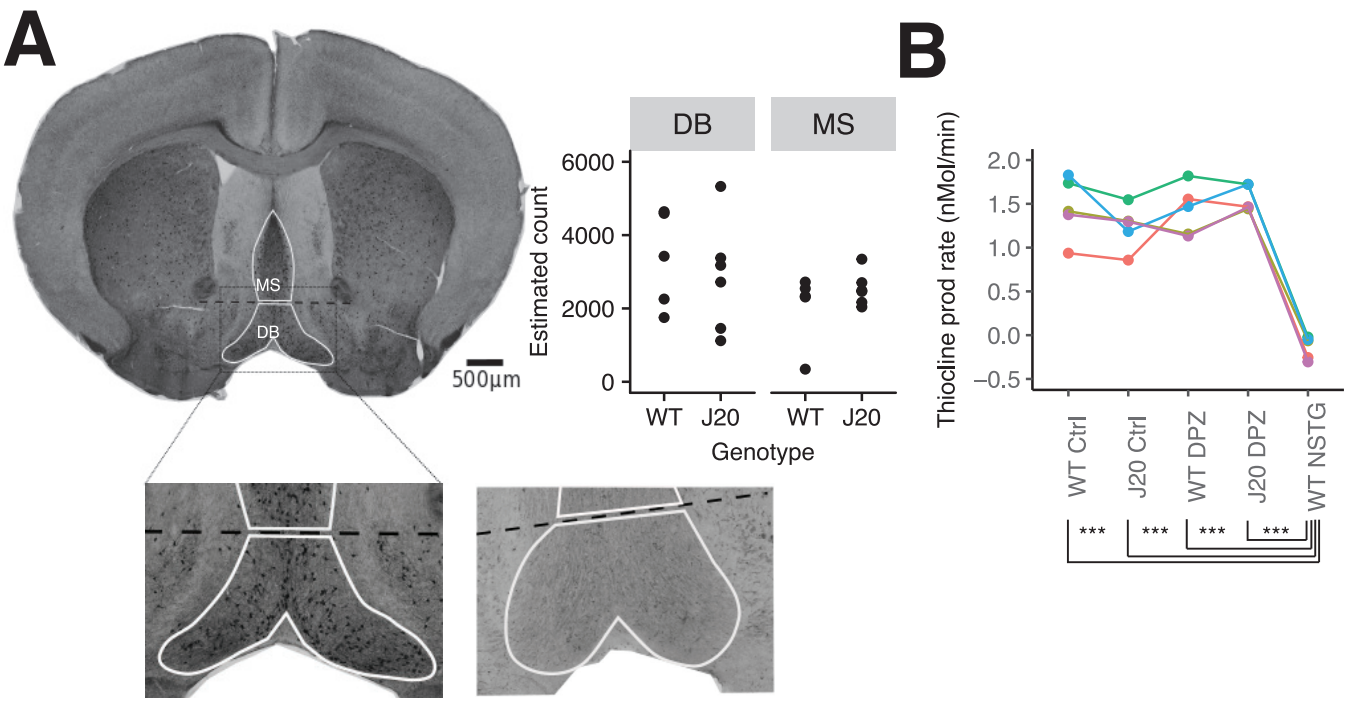

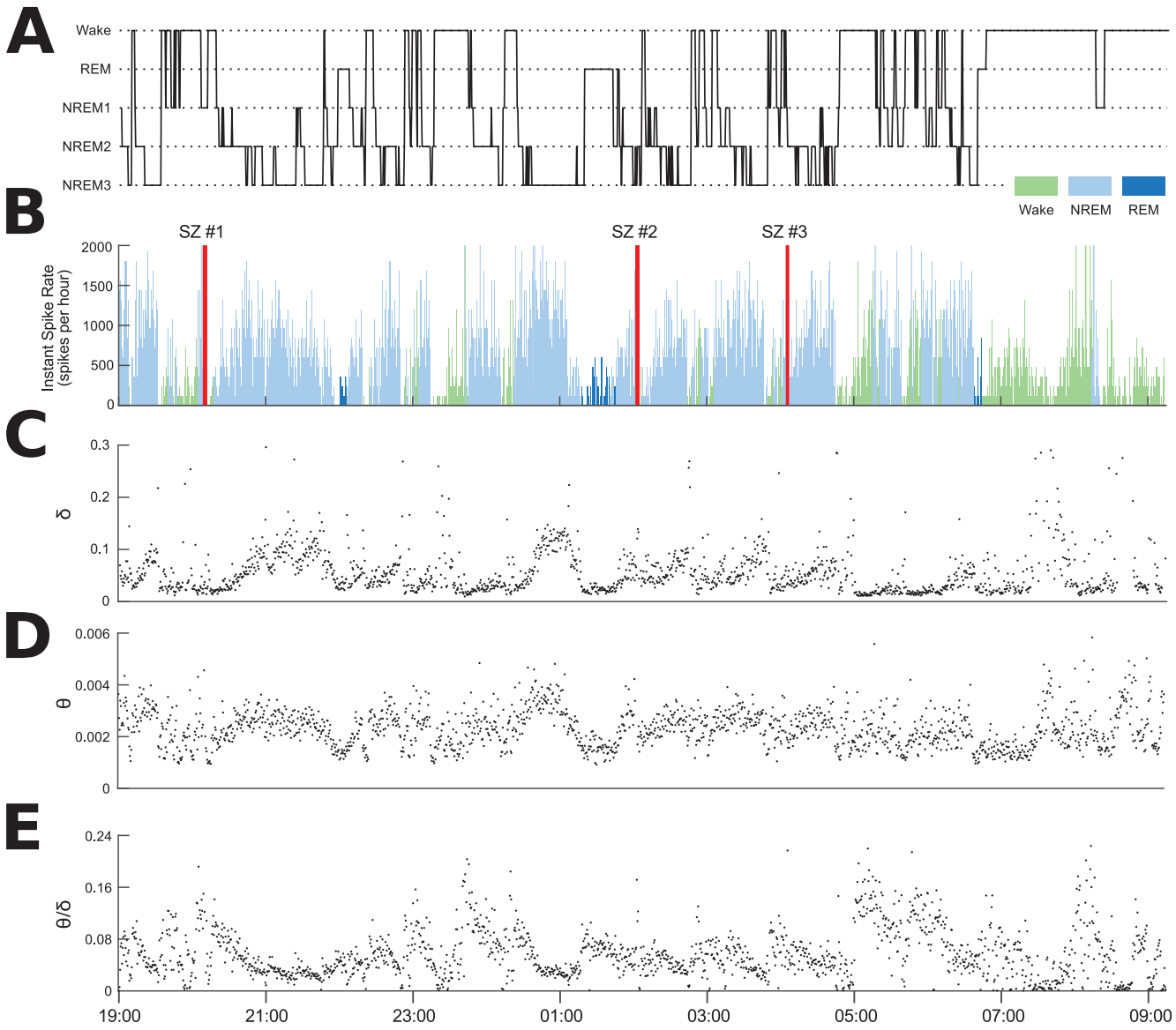

Table 1: Statistical table

	Data Structure	**Type of test**	**Confidence/ credible interval parameter**	**95% CI**
a	Normal (square root transformed)	t-test	Difference of means of square root data	(0.20, 0.30)
b	Normal (square root transformed)	Linear mixed model	β-Genotype β-Age	(-0.01. 0.03) (-0.02, -0.002)
c	IIS count data – (analysed with log-link function)	MCMC generalized model	Difference between estimates of θ/δ<1 vs. θ/δ>2. Provided for animals JF221, JF220, JF218, J0460, J0456, respectively	(1.619, 2.122) (0.261, 0.471) (0.254, 0.478) (1.166 ,1.392) (2.128, 2.372)
d	Normal (fourth root transformed)	Linear mixed model	β–□□□□□	(-0.004, 0.008)
e	Normal	Linear mixed model	β-Genotype	(-1015.7, 1029.0)
f	Non-normal	Wilcoxon -signed rank test	Difference of medians	(0.08, 0.65)

g	Normal (log transformed)	Tukey contrasts	J20_Ctrl - WT_Ctrl	(-0.24, 0.03)
			WT_DPZ - WT_Ctrl	(-0.15, 0.12)
			J20_DPZ - WT_Ctrl	(-0.08, 0.19)
			WT_NSTG - WT_Ctrl	(-1.50, -1.23)
			WT_DPZ - J20_Ctrl	(-0.04, 0.23)
			J20_DPZ - J20_Ctrl	(0.02, 0.29)
			WT_NSTG - J20_Ctrl	(-1.40, -1.13)
			J20_DPZ - WT_DPZ	(-0.07, 0.21)
			WT_NSTG - WT_DPZ	(-1.49, -1.22)
			WT_NSTG - J20_DPZ	(-1.56, -1.29)
h	Normal	Paired t-test	Difference of mean IIS rate	(-0.01, 0.03)

	Patient #1 (AD dementia)		Patient #2 (aMCI)	
Sleep Stage	Total Hours in Record	Average spike rate (spikes/hour)	Total Hours in record	Average spike rate (spikes/hour)
Wake	4.7	11	5.2	329
NREM1	0.7	31	1.5	670
NREM2	2.1	80	3.8	739
NREM3	1.4	62	3.1	903
REM	0	n/a	0.7	159